The Plant Cell, Vol. 17, 132–148, January 2005, www.plantcell.org

Receptor Salvage from the Prevacuolar Compartment Is Essential for Efficient Vacuolar Protein Targeting

Luis L.P. daSilva, J. Philip Taylor,[1] Jane L. Hadlington,[2] Sally L. Hanton,[3] Christopher J. Snowden, Sarah J. Fox, Ombretta Foresti, Federica Brandizzi,[3] and Jürgen Denecke[4]

Centre for Plant Sciences, Faculty of Biological Sciences, University of Leeds, Leeds LS2 9JT, United Kingdom

We have characterized the requirements to inhibit the function of the plant vacuolar sorting receptor BP80 in vivo and gained insight into the crucial role of receptor recycling between the prevacuolar compartment and the Golgi apparatus. The drug wortmannin interferes with the BP80-mediated route to the vacuole and induces hypersecretion of a soluble BP80-ligand. Wortmannin does not prevent receptor-ligand binding itself but causes BP80 levels to be limiting. Consequently, overexpression of BP80 partially restores vacuolar cargo transport. To simulate receptor traffic, we tested a truncated BP80 derivative in which the entire lumenal domain of BP80 has been replaced by the green fluorescent protein (GFP). The resulting chimeric protein (GFP-BP80) accumulates in the prevacuolar compartment as expected, but a soluble GFP fragment can also be detected in purified vacuoles. Interestingly, GFP-BP80 coexpression interferes with the correct sorting of a BP80-ligand and causes hypersecretion that is reversible by expressing a 10-fold excess of full-length BP80. This suggests that GFP-BP80 competes with endogenous BP80 mainly at the retrograde transport route that rescues receptors from the prevacuolar compartment. Treatment with wortmannin causes further leakage of GFP-BP80 from the prevacuolar compartment to the vacuoles, whereas BP80-ligands are secreted. We propose that recycling of the vacuolar sorting receptor from the prevacuolar compartment to the Golgi apparatus is an essential process that is saturable and wortmannin sensitive.

INTRODUCTION

Eukaryotic cells transport a range of proteins to several intracellular and extracellular destinations via the secretory pathway (Palade, 1975). The endoplasmic reticulum (ER) and the nuclear envelope are the sites where de novo–synthesized proteins enter the system, whereas the Golgi apparatus is responsible for protein sorting to the extracellular matrix, the plasma membrane, and the vacuolar compartments.

In plant cells, vacuoles are classified into lytic and storage vacuoles (Hoh et al., 1995; Paris et al., 1996; Bassham and Raikhel, 2000). However, it is not fully elucidated how the proper segregation of cargo molecules to the different types of vacuoles is mediated.

Transport to the lytic vacuole is thought to be receptor mediated (Kirsch et al., 1994, 1996; Humair et al., 2001) and occurs via clathrin-coated vesicles (CCVs) that bud from the Golgi apparatus and fuse with the prevacuolar compartment (PVC) (Sanderfoot et al., 1998; Li et al., 2002). The latter is probably the equivalent of the late endosome in mammalian cells and has recently been identified as the multivesicular body (Tse et al., 2004). Distinct early and late endosomes are also shown to exist in plants (Uemura et al., 2004) and will soon become accessible for routine analysis using emerging marker molecules.

Transport to the storage vacuole can occur via electron dense vesicles (DVs) that do not possess a recognizable protein coat (Chrispeels, 1983; Hohl et al., 1996). It is currently not known if DV-mediated transport is receptor mediated, but DVs were shown to segregate from CCVs starting from the *cis*-cisternae of the Golgi apparatus in pea (*Pisum sativum*) cotyledons (Hillmer et al., 2001). The existence of a direct route from the ER to the vacuole has also been proposed (Levanony et al., 1992; Hara-Nishimura et al., 1998; Toyooka et al., 2000), and again it is unclear whether cytosolic protein coats are involved and how the formation of such ER-derived carriers is regulated.

The search for plant vacuolar-sorting receptors has resulted in the discovery of one gene family encoding a type I membrane-spanning protein of 80 kD (BP80) via biochemical purification from plant CCVs. BP80 was shown to bind to a sequence-specific vacuolar sorting signal at pH 6.0 to 7.0 and to release it at pH 4.0 in vitro (Kirsch et al., 1994, 1996). The BP80 gene product exhibits the same membrane topology as the Vps10 gene product of yeast (*Saccharomyces cerevisiae*) (Marcusson et al., 1994) and appears to perform a similar function, although at the sequence level very little similarity with BP80 can be detected.

[1] Current address: Department of Biology, Coker Hall, CB#3280, University of North Carolina, Chapel Hill, NC 27599.
[2] Current address: QIAGEN, Fleming Way, Crawley, West Sussex, RH10 9NQ, UK.
[3] Current address: Department of Biology, University of Saskatchewan, Saskatoon, SK S7N 5E2, Canada.
[4] To whom correspondence should be addressed. E-mail j.denecke@leeds.ac.uk; fax 44-113-3432835.
The author responsible for distribution of materials integral to the findings presented in this article in accordance with the policy described in the Instructions for Authors (www.plantcell.org) is: Jürgen Denecke (j.denecke@leeds.ac.uk).
Article, publication date, and citation information can be found at www.plantcell.org/cgi/doi/10.1105/tpc.104.026351.

Further research has established that BP80 is localized to the Golgi apparatus, CCVs, and the PVC but is not present in DVs (Ahmed et al., 1997, 2000; Paris et al., 1997; Sanderfoot et al., 1998; Hinz et al., 1999; Hillmer et al., 2001; Li et al., 2002; Tse et al., 2004).

Evidence for BP80-ligand interaction in vivo was first presented through cross-linking studies (Miller et al., 1999) and the vacuolar delivery of plant vacuolar cargo to the yeast vacuole in Vps10 mutants overexpressing BP80 (Humair et al., 2001). Most recently, gene-knockout experiments demonstrated the involvement of one BP80 gene family member in the transport of storage proteins to the vacuoles (Shimada et al., 2003), whereas an ER-retained soluble derivative of the pumpkin (*Cucurbita* sp cv Kurokawa Amakuri Nankin) BP80 gene family member PV72 prevented vacuolar delivery of a typical cargo for the lytic vacuole (Watanabe et al., 2004). The combined results suggest that the BP80 gene family is not exclusively responsible for targeting to the lytic vacuole but may have a more general role.

Wortmannin, a drug that inhibits phosphatidylinositol 3-kinase activity in mammalian cells (Thelen et al., 1994) and additionally inhibits phosphatidylinositol 4-kinase activity in plant cells, has been used to differentiate between two vacuolar sorting routes (Matsuoka et al., 1995). The drug was shown to inhibit the vacuolar sorting of proteins carrying C-terminal sorting signals but not those with sequence-specific sorting signals. However, further research revealed that the sequence-specific vacuolar sorting route is also strongly inhibited by wortmannin (Kim et al., 2001; Pimpl et al., 2003).

Here, we show that wortmannin inhibits the recycling of BP80 from the PVC and that this route can also be saturated by increasing the dosage of molecules containing the BP80 transmembrane domain and cytosolic tail. The importance of the PVC as a salvage organelle for vacuolar sorting receptors is discussed.

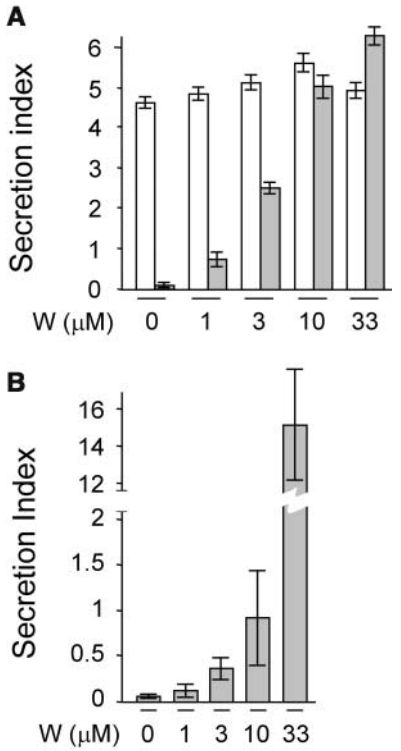

Figure 1. Wortmannin Strongly Inhibits the Sequence-Specific Vacuolar Sorting Route.

(A) The concentration-dependent influence of the drug wortmannin on the secretion index of amy (white bars) and amy-spo (gray bars) in tobacco mesophyl protoplasts. Transcriptional control of the cargo proteins was driven by the 35S promoter of *Cauliflower mosaic virus* (pCaMV35S), and 3′ end processing and polyadenylation was controlled by the 3′ untranslated end of the nopaline gene (3′nos). Protoplasts were transfected with a constant amount (10 μg) of plasmid-encoded cargo molecule and distributed in equal portions, subject to different concentrations of wortmannin and incubated for 24 h after which cells and media were harvested. The concentration of the drug is given below each lane. The secretion index was calculated as the ratio between the extracellular and the intracellular amy activities (Phillipson et al., 2001).

(B) The concentration-dependent influence of the drug wortmannin on the secretion index of amy-spo in transgenic tobacco BY2 cells. Because of the very high secretion index at 33 μM wortmannin, a split *y* axis was used for this lane.

RESULTS

Wortmannin Causes Secretion of BP80-Ligands

It has been shown previously that wortmannin causes hypersecretion of soluble cargo molecules carrying a sequence-specific vacuolar sorting signal (Kim et al., 2001; Pimpl et al., 2003). Because this deviated substantially from previous findings (Matsuoka et al., 1995), we have systematically compared the effects of an increasing concentration of wortmannin on vacuolar sorting. The secretory protein α-amylase (amy) was compared with an amy fusion protein carrying the sequence-specific sorting signal of sweet potato (*Ipomoea batatas*) sporamin (amy-spo). The latter fusion has been extensively tested and described previously (Pimpl et al., 2003), and the sequence-specific nature has been further confirmed by a control experiment in which addition of two glycin residues to the C terminus does not affect its functionality (see Methods).

To test the effect of the drug on the cargo molecules, tobacco (*Nicotiana tabacum*) leaf protoplasts were transfected, pooled, and split into equal portions and incubated either without the drug or with increasing concentrations of wortmannin as indicated below each lane (Figure 1A). After analyzing cells and medium, the ratio between the extracellular and intracellular enzyme activity was calculated and is shown as the secretion index (Phillipson et al., 2001; Pimpl et al., 2003). The results show that hardly any effect of the drug was observed for the secretory marker amy as reported before (Pimpl et al., 2003). By contrast, wortmannin caused a substantially induced secretion for amy-spo in a dosage-dependent fashion.

To test if the drug exhibits a different effect in different cell types, we analyzed BY2 cells that were stably transformed with amy-spo. Figure 1B shows that BY2 cells exhibited a similar if not higher sensitivity to the drug as visualized by a drastically

induced secretion index of amy-spo. Again, the effect is dosage dependent, and the sorting of amy-spo cannot be regarded as insensitive or resistant to wortmannin at any of the concentrations used. This is in contrast with a previous report on the effect of the drug on sweet potato sporamin in BY2 cells (Matsuoka et al., 1995).

To confirm amy-spo as a BP80-ligand, we took advantage of the fact that a soluble luminal portion of BP80 fused to a C-terminal HDEL motif was shown to retard vacuolar delivery of soluble ligands (Watanabe et al., 2004). Chimeric genes were constructed encoding soluble derivatives devoid of the transmembrane domain and cytosolic tail of *Arabidopsis thaliana* BP80a (U79960, At2g14720). This gene family member was chosen because it is the Arabidopsis isoform most related to pea BP80 (Hadlington and Denecke, 2000; Paris and Neuhaus, 2002). The chimeric constructs included a C-terminal myc tag for detection, and transient expression confirmed that the HDEL-tagged BP80a (sBP80a-HDEL) is efficiently retained in the cells (Figure 2A) in contrast with the secreted-soluble BP80a (sBP80a). To test the effect of BP80a-HDEL rapidly and quantitatively, transfected cells were fractionated into soluble proteins released by osmotic shock (S1) and proteins released after sonicating the pellet (S2). The first fraction is enriched in cytosolic and vacuolar solutes, whereas the second is enriched in microsomes derived from the ER, the Golgi apparatus, and the endosomes (Denecke et al., 1992). Figure 2B shows that coexpression of sBP80a-HDEL causes a dosage-dependent shift of the intracellular partitioning of amy-spo from S1 to S2, whereas a control cargo (amy-spoM) containing a mutagenized sorting signal (Pimpl et al., 2003) failed to exhibit such a redistribution. This result provides positive evidence that amy-spo is a BP80a-ligand and illustrates the use of the engineered BP80 derivative (Watanabe et al., 2004).

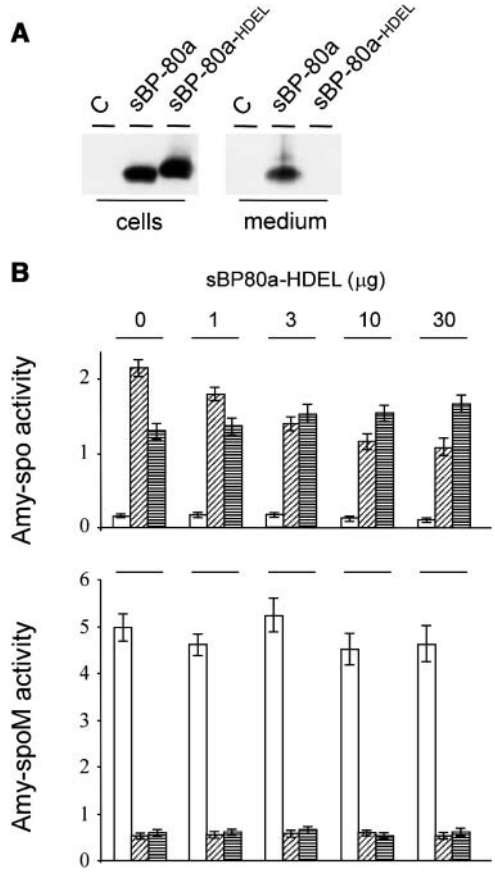

Figure 2. Confirmation of amy-spo as a BP80-Ligand in Vivo.

(A) Transport assay for soluble BP80 molecules with or without the ER retention motif HDEL via transient expression in tobacco protoplasts. Shown is a protein gel blot of cells and medium from untransformed (C) and transfected cells with 10 μg of plasmid-encoded pCaMV35S: sBP80a-myc:3′nos or a C-terminal HDEL-fused version (sBP80a and sBP80a-HDEL, respectively). After 24-h incubation, cells and medium were harvested and analyzed via protein gel blot to investigate the steady state distribution of the chimeric proteins. Proteins were detected using anti-myc antiserum.

(B) sBP80a-HDEL mediates specific subcellular redistribution of amy-spo. Protoplasts were transfected with a constant amount (10 μg) of plasmid encoding either amy-spo or the control cargo amy-spoM (Pimpl et al., 2003), in which the vacuolar sorting signal is mutated. An increasing amount of plasmid-encoded sBP80a-HDEL (as indicated above each lane) was cotransfected. Cells and medium were harvested as in Figure 1, but the cell fraction was further partitioned into soluble proteins released after osmotic shock (S1), which is enriched in cytosolic and vacuolar solutes and soluble proteins released after sonication of the S1-free pellet (S2). The latter fraction is enriched in microsomal proteins. The amy activity was calculated for each fraction and shown as follows: medium (white bars), S1 (diagonally striped bars), and S2 (horizontally striped bars). amy activity is given in ΔOD per mL and per min reaction time.

Wortmannin Does Not Prevent Ligand Binding to BP80

To investigate how wortmannin causes hypersecretion of BP80-ligands, we first tested if the drug interferes with the physical interaction between BP80 and its ligands. Therefore, we used the simple sBP80a-HDEL–mediated in vivo receptor binding assay with wortmannin-treated cells. If receptor–ligand interactions still occur in wortmannin-treated cells, coexpression of sBP80a-HDEL should reduce the secretion of amy-spo. Figure 3A shows that wortmannin-induced secretion of amy-spo is indeed inhibited by sBP80a-HDEL. Importantly, no effect on secretion was observed with the secretory control cargo amy. Therefore, the drug does not seem to interfere with ligand binding directly.

To further explore how wortmannin targets the BP80 route, we tested if full-length BP80a overexpression could cause a degree of resistance to the drug. Figure 3B shows that it was possible to overexpress and detect BP80a in tobacco protoplasts, as illustrated by an increase in the BP80 signal in microsomal fractions. The control marker calnexin confirmed that equal levels of microsomes were loaded.

We then tested the effect of increasing amounts of full-length BP80a in wortmannin-treated tobacco protoplasts expressing either amy or amy-spo. Figure 3C shows the relative effect of cotransfected full-length BP80a in a constant background of 10 μM wortmannin. The result demonstrates that increasing concentrations of full-length BP80a significantly reduces the secretion of amy-spo, the predicted BP80-ligand. By contrast, no meaningful effect is observed with the secretory cargo amy. As in Figure 2, this is an important control because it highlights the

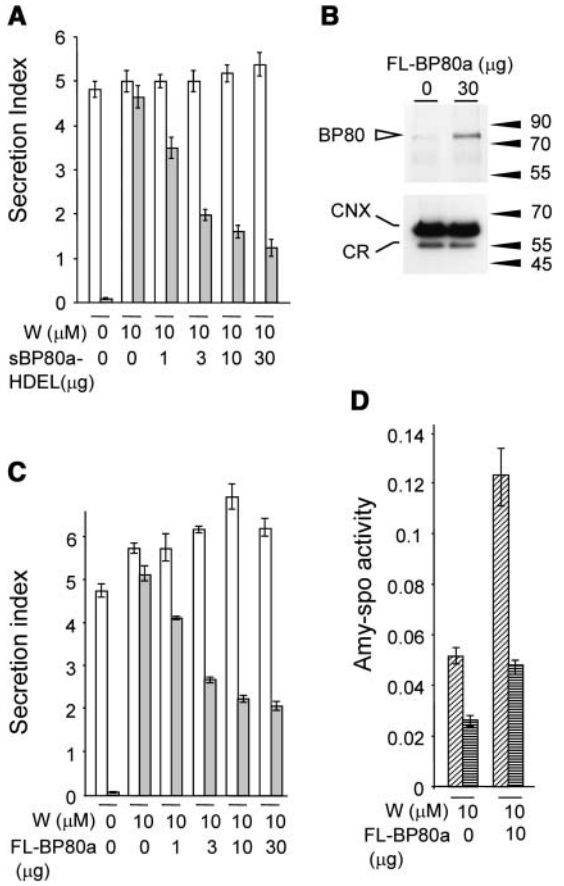

Figure 3. Wortmannin Does Not Prevent BP80-Ligand Interactions.

(A) Wortmannin does not prevent BP80 from physically interacting with its ligands. Protoplasts were transfected with either amy or amy-spo, together with increasing concentrations of sBP80-HDEL plasmid preparation (as stated below each lane) and were incubated for 24 h with a constant concentration of wortmannin (10 μM) as indicated. The amy activity was obtained for each fraction, and the secretion index was calculated and compared for each cargo: amy (white bars) and amy-spo (gray bars).

(B) Microsomal fractions from mock transfected and transfected protoplasts to test if transient expression of plasmid-encoded pCaMV35S: full-length BP80a:3′nos (FL-BP80a) is detectable. The amount of FL-BP80a plasmid is indicated above the lane. Molecular mass markers are indicated in kD. The top panel shows a protein gel blot probed with anti-AtBP80 antiserum (Laval et al., 1999), which had been subtracted as described in Methods. Notice the strongly induced band at ~80 kD in microsomes from transfected protoplasts. The bottom panel shows a protein gel blot probed with anticalnexin antibodies (Pimpl et al., 2000, 2003) that binds to calnexin (CNX) and calreticulin (CR). This illustrates that equal levels of total microsomes were loaded in both lanes.

(C) Reconstitution of BP80-mediated sorting by coexpression of full-length BP80a. Protoplasts were transfected with a constant amount of cargo molecules and a dilution series of the same FL-BP80a plasmid preparation used for **(B)** and incubated within a constant wortmannin background (10 μM). As in **(A)**, a control lane with cargo alone was included without wortmannin to illustrate the degree of secretory induction for each cargo molecule. Notice that the addition of FL-BP80a partially reverses the effect of wortmannin on amy-spo but not amy secretion.

specificity of the in vivo assay and demonstrates that BP80a overexpression does not cause a general inhibition of anterograde traffic.

To test if overexpressed full-length BP80a promotes vacuolar sorting and not just cell retention in wortmannin-treated cells, we analyzed S1 and S2 fractions. The results show that overexpressed BP80a leads to an increased amy-spo level in both cell fractions (Figure 3D). Thus, additional BP80a molecules are not merely trapping amy-spo in the early secretory pathway, but a large proportion proceeds to the vacuole. The results suggest that higher numbers of BP80a molecules reverse the wortmannin-induced secretion of BP80-ligand amy-spo. We postulate that the drug causes BP80 molecules to be the limiting factor for vacuolar sorting rather than interfering with ligand binding directly.

Inhibition of Vacuolar Sorting by Coexpression of a Truncated Receptor

To study BP80-dependent transport further, BP80 derivatives were constructed in which the entire lumenal ligand binding domains were replaced by green fluorescent protein (GFP) (Figure 4A). We have used the Arabidopsis isoforms BP80a (U79960; At2g14720), BP80b (U86700; At3g52850), also known as AtELP, which has been studied most in recent years (Ahmed et al., 1997, 2000; Shimada et al., 2003), BP80d (NM_102827; At1q30900), and BP80f (NM_118130; At4q20110) as classified previously (Hadlington and Denecke, 2000; Paris and Neuhaus, 2002; Laval et al., 2003). It was shown previously that the transmembrane domain and cytosolic tail of pea BP80 are sufficient to transport aleurain to a lytic compartment in which propeptide processing occurs (Jiang and Rogers, 1998). Moreover, the same domains target yellow fluorescent protein (YFP) to the PVC and colocalizes with endogenous BP80 (Tse et al., 2004). It could thus be predicted that the new GFP-BP80 fusions would compete with endogenous BP80 for sorting machinery. Moreover, because of its inability to bind ligands, the fusion protein would occupy limiting sites within transport vesicles and thus compromise vacuolar sorting.

To test that any effect observed with GFP-BP80 fusions was specifically because of the BP80 domains present in the fusion protein, a control construct was created in which the transmembrane domain and cytosolic tail of BP80 were replaced by the equivalent portion of calnexin. The resulting chimeric gene (GFP-calnexin) has the same topology and almost identical dimensions to the GFP-BP80 fusions. Further controls included secreted GFP and a GFP fusion with the sweet potato sporamin propeptide (GFP-spo).

(D) Overexpression of full-length BP80a leads predominantly to vacuolar transport of amy-spo. Protoplasts expressing amy-spo with or without FL-BP80a were incubated with 10 μM wortmannin, after which cells were isolated and fractionated into S1 and S2, similarly as in Figure 2. amy-spo activity was measured for each fraction and compared: S1 (diagonally striped bars) and S2 (horizontally striped bars).

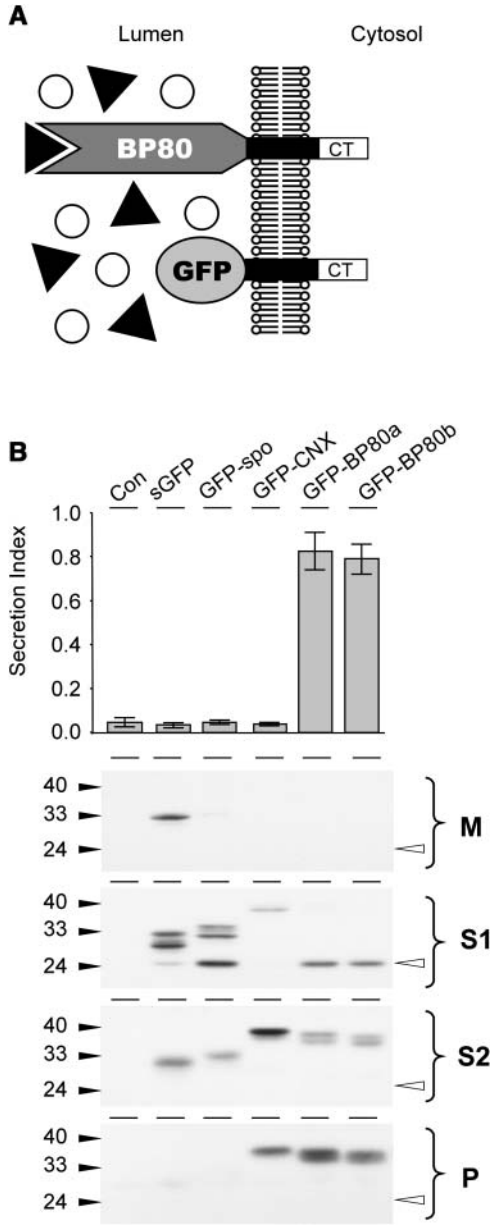

Figure 4. Truncated BP80 Lacking the Ligand Binding Domain Interferes with Vacuolar Sorting.

(A) Schematic illustration of the nature and topology of the truncated BP80 fusions in relation to the full-length BP80. The complete ligand binding domain of the Arabidopsis BP80 isoforms a, b, d, and f (Hadlington and Denecke, 2000) were replaced by GFP, which results in the truncated molecules (GFP-BP80a, GFP-BP80b, GFP-BP80d, and GFP-BP80f) that do not interact with BP80-ligands but yet display the same polypeptide on the cytosolic face of the membrane as the wild-type BP80 counterparts.

(B) Protoplasts were transfected with plasmid-encoding amy-spo alone or together with 20 μg of plasmid encoding either sGFP, sGFP-spo, GFP-calnexin (GFP-CNX), or GFP-BP80 fusions (represented here by GFP-BP80a and b) and incubated for 24 h, after which medium and cells were harvested. The top panel shows the secretion index of cotransfected amy-spo; annotations are as in the previous figures. Notice that only GFP-BP80a and GFP-BP80b induce the secretion of amy-spo, whereas sGFP, GFP-spo, and GFP-CNX have no effect. Cells were fractionated to obtain extracts enriched in soluble protein released by osmotic shock (S1), proteins released after sonicating the first pellet (S2), and membrane spanning proteins (P). These cell fractions together with the medium (M) were analyzed (bottom panel) to test the intracellular partitioning of the various GFP fusions. Molecular mass markers are indicated in kD. Notice the lower molecular mass degradation fragment, the GFP core (white arrowhead) that is detected exclusively in S1 for all GFP fusions except for GFP-CNX.

The various constructs were cotransfected with amy-spo, and the culture medium and cells were harvested after 24 h. We first tested the effect of coexpressed GFP fusions on the sorting of amy-spo. Figure 4B shows that the two BP80 fusions GFP-BP80a and GFP-BP80b strongly induced the secretion of amy-spo, similar to the drug wortmannin. The same was observed for the other fusions carrying the equivalent domains of isoforms d and f (data not shown). The induced secretion of amy-spo is not because of a general effect of overexpressing a type I membrane protein because GFP-calnexin does not influence the sorting of amy-spo. Also, the two soluble GFP cargo molecules did not significantly affect amy-spo sorting (Figure 4B).

To analyze the GFP fusions, cells were fractionated into extracts enriched in soluble proteins and membrane proteins to test intracellular partitioning. As in Figure 2, soluble proteins were partitioned into those released by osmotic shock (S1) and those released after sonicating the first pellet (S2). In addition, the second pellet was enriched in membrane-spanning proteins and was analyzed as well. Figure 4B shows that all GFP fusions produce multiple bands. This is partially because of the use of a glycosylated-GFP derivative (Batoko et al., 2000) but also because of proteolysis.

Secreted GFP was found to be soluble and secreted, whereas GFP-spo was hardly detected in the medium and mainly fractionated with the first soluble fraction (S1). Interestingly, a lower molecular weight degradation fragment was seen, identical to a band previously described (Frigerio et al., 2001; Brandizzi et al., 2003; Sohn et al., 2003) and hereafter termed the GFP core. The GFP core is never detected in the culture medium and is much more intense for GFP-spo compared with GFP alone. The results confirm that a small proportion of secreted GFP reaches a lytic compartment, but this is greatly increased by the addition of a vacuolar sorting signal. Interestingly, all the membrane-spanning GFP fusions also exhibited substantial levels of this degradation product, except for the calnexin fusion. In each case, the GFP core has the same molecular weight and partitions exclusively to the S1 fraction, which contains cytosol and vacuolar lumen and only minor portions of microsomes. As expected, the full-length molecules also strongly partition into the microsomal S2 fraction, which contains not only microsomal lumen but also sonicated membrane fragments that failed to sediment. However, only the three membrane-spanning proteins partition into the final membrane-enriched pellet.

The results suggest that unlike the calnexin fusion, GFP-BP80 fusions reach a lytic compartment in which processing to the

GFP core can occur supporting previous observations with another reporter (Jiang and Rogers, 1998). None of the GFP bands of the membrane fusions were detected in the culture medium, which suggests that the soluble degradation product of GFP-BP80 must be generated after the compartment from which export to the cell surface occurs. A control experiment using the glycosylation inhibitor tunicamycin confirms the upper two bands as glycosylated and unglycosylated full-length fragments (data not shown).

Truncated BP80 Competes with Endogenous BP80 and Inhibits Vacuolar Sorting of a BP80-Ligand

The results obtained so far show that overexpression of GFP-BP80 fusions leads to their missorting to the vacuoles and causes induced secretion of amy-spo. To confirm a specific effect on vacuolar transport of soluble ligands, we have compared the influence of GFP-BP80a coexpression for three soluble cargo molecules: amy, amy-HDEL, and amy-spo. In addition, a construct expressing the cytosolic protein β-glucuronidase (GUS) (Leborgne-Castel et al., 1999) was used to test for increased cell mortality. Cells were transfected with a constant amount of plasmid encoding each of the cargos with a dilution series of the effector GFP-BP80a.

Figure 5A shows that the chimeric construct strongly inhibits the vacuolar sorting of the BP80-ligand (amy-spo), as indicated by an approximate 30-fold increase in the secretion index at the highest concentration of GFP-BP80a (compare lane 1 with lane 6). In the case of the secretory control (amy), hardly any effect was seen. The secretion index of amy-HDEL was slightly reduced (Figure 5B), and the cytosolic protein GUS was tested and found to be present at ~2 to 3% of the total activity in the medium (secretion index of 0.02 to 0.03) regardless of the concentration of GFP-BP80a. These two additional controls indicate that increased cell mortality can be ruled out as a cause for induced secretion of amy-spo.

To confirm that GFP-BP80a competes with endogenous tobacco BP80 for transport machinery, we tested if coexpression of full-length BP80a could alleviate the effect. For this purpose, an intermediate level of GFP-BP80a was electroporated with a constant amount of cargo-encoding plasmid, together with a dilution series of plasmid encoding full-length BP80a. Figure 5C shows that coexpression of wild-type BP80a counteracts the effect of truncated BP80a in a dosage-dependent manner. A 10-fold excess of wild-type BP80a almost completely alleviated the inhibition by the chimera. The control cargo amy was not influenced by coexpression of GFP-BP80a, and increasing concentrations of wild-type BP80a did not cause any change either. This shows that only BP80-ligands are influenced by this in vivo assay.

Increasing BP80a expression neither affected the total cargo levels nor the quantity of the effector molecule GFP-BP80 produced (bottom panels of Figure 5C). This indicates that GFP-BP80a and full-length BP80 specifically compete with each other. This is quite distinct from the dominant-negative poisoning of the pathway observed for mutants of the GTPase ARF1 for instance (Pimpl et al., 2003).

Wortmannin Causes Increased Leakage of GFP-BP80 to the Vacuole

Our data suggest that GFP-BP80 fusions (Figure 4) compete with tobacco BP80 for sorting machinery needed to sustain traffic between the Golgi apparatus and the PVC. The reconstitution of vacuolar sorting by full-length BP80 as well as the presence of the soluble GFP core suggest that the limiting factor is likely to be the rescue from the PVC. Endogenous BP80 molecules could thus be lost when GFP-BP80 is coexpressed. To test this, we studied the subcellular localization of GFP-BP80 and the influence of wortmannin on this fusion protein.

Protoplasts were transfected with the GFP-BP80 fusions, and as a Golgi marker, a chimeric construct was cotransfected, which carries the spectral variant YFP fused to the transmembrane domain of sialyl transferase (ST-YFP) (Brandizzi et al., 2002). In vivo imaging revealed that all GFP-BP80 fusions labeled punctate structures of more variable size and often smaller than the typical Golgi bodies highlighted by ST-YFP (Figures 6A and 6B). GFP-BP80–labeled structures are often Golgi associated but clearly physically separated. Hardly any colocalization was seen between the two markers, which corresponds with observations that BP80 accumulates predominantly in the PVC (Li et al., 2002; Tse et al., 2004). GFP-BP80 structures were equally mobile as Golgi bodies but moved independently when observed over long periods of time. Only at very high expression levels could some colocalization with the Golgi marker be observed, but the predominant signals still arise from extra-Golgi structures (data not shown). This strongly suggests that anterograde transport is not the limiting factor in GFP-BP80–mediated inhibition of vacuolar sorting, and considering the current state of the art in the field (Tse et al., 2004), we have defined the GFP-BP80 structures as PVC.

We have obtained the same results with GFP-BP80d (Figure 6B) and the two other fusions carrying the domains from isoforms BP80d and BP80f (data not shown). Detailed investigations to test if the various domains from the isoforms carry differential sorting information failed to reveal any difference so far, and all fusions exhibit the same effect on the control cargo amy-spo (Figure 4).

A weak fluorescence in the vacuolar lumen was also detected for GFP-BP80 fusions but is not easily seen with optical sections of intact protoplasts (Figure 6C, control). However, upon treatment with wortmannin, the vacuolar fluorescence increased noticeably, whereas the GFP-BP80–labeled PVC structures decreased in number and intensity (Figure 6C, wortmannin). This was observed for all fusion proteins, and all further experiments were conducted with GFP-BP80a. In purified-vacuole preparations from wortmannin-treated cells, fluorescence was easily seen and was absent in vacuoles from untransfected cells (Figure 6D). The presence of nonfluorescent vacuoles, originating from untransfected protoplasts, rules out that wortmannin induces a general green autofluorescence in vacuoles. We conclude that the drug specifically causes a redistribution of GFP-BP80 from the PVC toward the vacuole in transfected protoplasts.

To strengthen the experimental evidence further, we tested if wortmannin-induced missorting to the vacuole could also be observed biochemically by an increase in the level of the soluble GFP core (Figure 4B). Protoplasts were transfected with

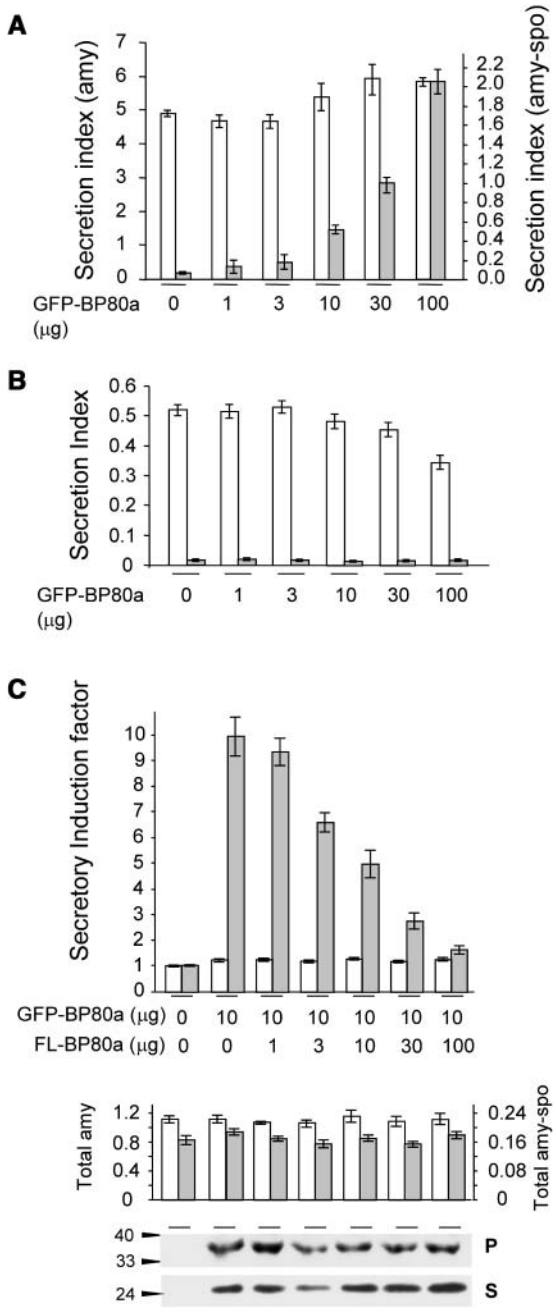

Figure 5. Truncated BP80 Is Codominant versus Full-Length BP80.

(A) The concentration-dependent influence of GFP-BP80 coexpression on the secretion index of amy and amy-spo in tobacco mesophyl protoplasts. Protoplasts were transfected with constant levels of plasmids encoding each of the cargo molecules together with a dilution series of plasmid-encoding GFP-BP80a. The secretion index is given in different scales for amy (left *y* axis) and amy-spo (right *y* axis) to simplify comparison. Notice that the effector molecule exhibits a wortmannin-like effect (compare with Figure 1A) specifically for amy-spo (gray bars) but not amy (white bars). Dosage-dependent expression of effector molecules was routinely tested by anti-GFP–probed protein gel blots from total cell extracts (data not shown).

(B) Control experiments using cell-retained amy-HDEL (white bars) and cytosolic GUS (gray bars) to test nonspecific cell leakage. Experimental conditions and annotations are as in **(A)**. Notice that GFP-BP80 does not cause an induced secretion index for these two control molecules.

(C) Transient expression experiment to test if full-length BP80a (FL-BP80a) and truncated BP80a compete with each other. Protoplasts were transfected with a constant amount of plasmid (10 μg) encoding either amy or amy-spo, together with a constant amount of plasmid encoding GFP-BP80a and a dilution series of plasmid encoding FL-BP80a from the same batch as used in Figure 2. The amount of effector plasmid DNA is indicated below each lane. The secretion index was calculated as previously, and the secretory induction factor is calculated for amy-spo (gray bars) and amy (white bars) by dividing each value by the respective secretion index for the control lane (without GFP-BP80a and without FL-BP80a). The second panel shows the total activities for amy (white bars) and amy-spo (gray bars) in the corresponding lanes. The bottom panel shows the levels of GFP-BP80a precursor in the pellet fraction (P) and soluble GFP core in the soluble fraction (S) for each corresponding lane.

GFP-BP80a and incubated for 22 h to reach a steady state distribution, after which the population was split into equal portions and incubated with wortmannin for different times (Figure 7A).

The protein gel blot shows that wortmannin causes a rapid decline of the full-length precursor form and a simultaneous increase in the soluble GFP core. A control experiment without wortmannin (Figure 7B) did not show any redistribution in the same time frame, confirming that steady state levels were reached after 22 h. A second control experiment with GFP-calnexin failed to yield any form of degradation product even in the presence of wortmannin. In addition, the amount of the full-length GFP-calnexin fusion protein in the membrane fraction did not decline over time (Figure 7C). This shows that BP80 sequences, either in the transmembrane domain or the cytosolic tail, are required to yield wortmannin-induced missorting to the vacuole.

To test if the wortmannin-induced GFP-BP80 degradation product was actually localized in the vacuoles, we compared the signals from total cells with those of purified vacuoles (Figure 8A). The data clearly demonstrate that the GFP core copurifies with vacuoles in contrast with the higher molecular weight precursors. GFP core is present in vacuoles before the treatment, but its levels increase steadily with time after adding wortmannin.

The PVC has previously been shown to exhibit a higher density than Golgi membranes in sucrose gradients (Tse et al., 2004) and would pellet together with the ER and the Golgi through a 20% sucrose cushion after ultracentrifugation. Thus, obtained microsomal preparations from cells incubated with or without wortmannin for 4 h failed to yield detectable levels of the GFP core fragment. This suggests that premature processing in the PVC is unlikely to occur, regardless of the presence of the drug. Large quantities of microsomes were loaded, and even if transport from the endosomes is rapid, a portion of the GFP core should have been detectable if it existed in this fraction. Endogenous calnexin did not copurify with the vacuoles, illustrating the purity of the vacuolar fraction. Likewise, calnexin levels were identical in the three microsomal preparations, confirming loading of equivalent fractions.

To exclude that increased levels of vacuolar degradation products are because of a wortmannin-induced change in the

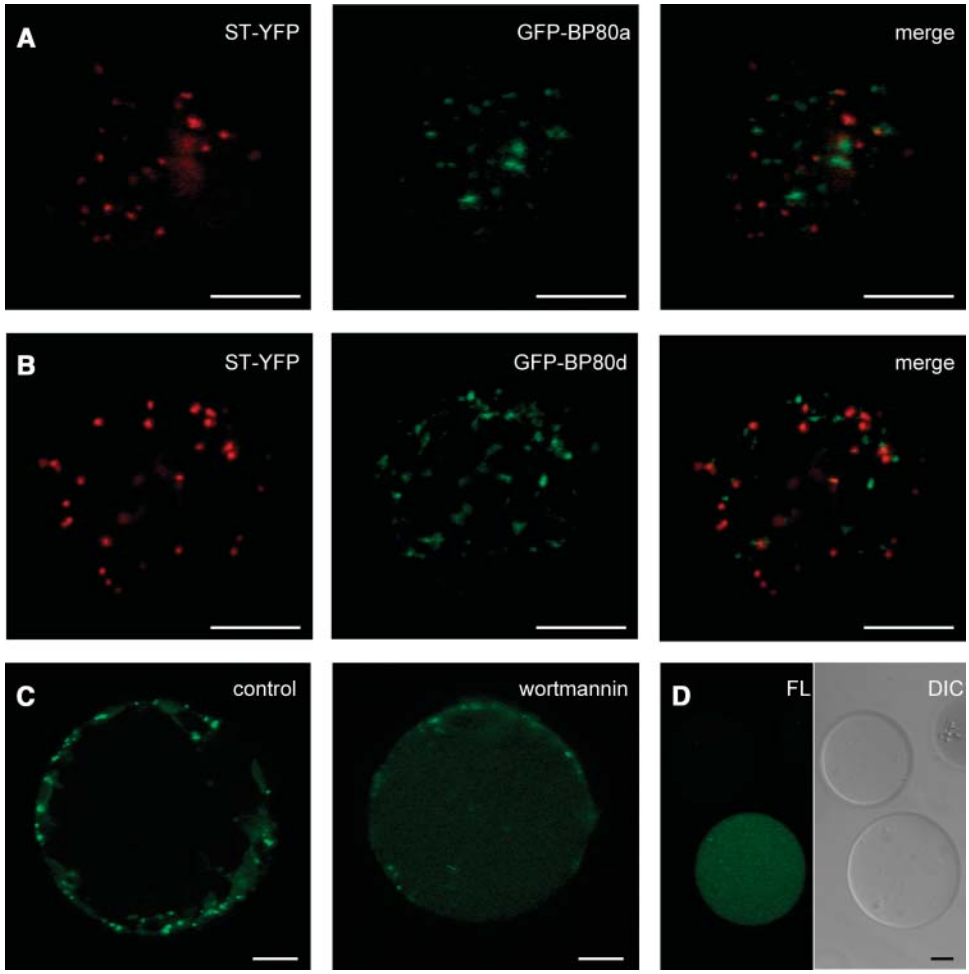

Figure 6. Confocal Laser Scanning Microscopy Demonstrating Increased Vacuolar Sorting of GFP-BP80 by Wortmannin.

(A) Protoplasts were cotransfected with 10 μg of plasmids encoding GFP-BP80a and the Golgi marker ST-YFP, live-embedded in TEX medium with 1% low melting agarose, and incubated for 24 h. The images present a 2.5-μm optical section through the cell cortex to give a view of the cytosol with the intermediate organelles of the secretory pathway. ST-YFP labels Golgi bodies (pseudocolored in red), and GFP-BP80a (pseudocolored in green) labels punctuate structures. Notice that hardly any overlap with the Golgi was detected (merge, colocalization is pseudocolored in yellow).
(B) The same as **(A)** but with transfection of GFP-BP80d instead of GFP-BP80a. Note the very similar pattern as is visualized for this BP80 derivative from another family member (compare panels **[A]** and **[B]**), which is also the case when using the derivatives from isoforms b and f (data not shown).
(C) Protoplasts were transfected with plasmid-encoding GFP-BP80a and incubated for 22 h in liquid TEX medium, after which protoplasts were washed, concentrated, and incubated for another 2 h in control conditions or in the presence of 10 μM wortmannin. Shown is a cross section through the center of the protoplast to appreciate the vacuole lumen. Notice that upon wortmannin treatment, punctuate fluorescence at the cell cortex diminishes, whereas diffuse fluorescence in the vacuole lumen increases.
(D) Isolated vacuoles from the same protoplast suspension presented in **(C)** (+ wortmannin) and analyzed by confocal laser scanning microscopy in bright field (differential interference contrast [DIC]) and the green fluorescent channel (FL). Notice that wortmannin-induced vacuolar fluorescence does not occur in all vacuoles and is restricted to vacuoles isolated from transfected cells.
Bars in **(A)** to **(D)** = 10 μm.

vacuolar pH, a control experiment was performed in which a GFP-sporamin fusion, which yields an identical vacuolar GFP core fragment (Figure 4B), was tested. Figure 8B shows that GFP-spo–expressing protoplasts at steady state (22 h) show a rapid reduction of the GFP core level upon treatment with the drug for 4 h. Statistical analysis of 100 purified vacuoles from either GFP-BP80 or GFP-spo–expressing cells (Figure 8C) revealed that wortmannin reduced the vacuolar fluorescence derived from GFP-spo and increased the fluorescence derived from GFP-BP80a. The result illustrates that pH changes are unlikely to cause the wortmannin-induced differential effect on GFP-spo and GFP-BP80–derived GFP core fragments in the vacuoles.

The experiments in the previous section were conducted with protoplasts exhibiting steady state levels of GFP-BP80 fusion proteins, which predominantly localized to the PVC but redistributed rapidly to the vacuoles. To test the opposite behavior of

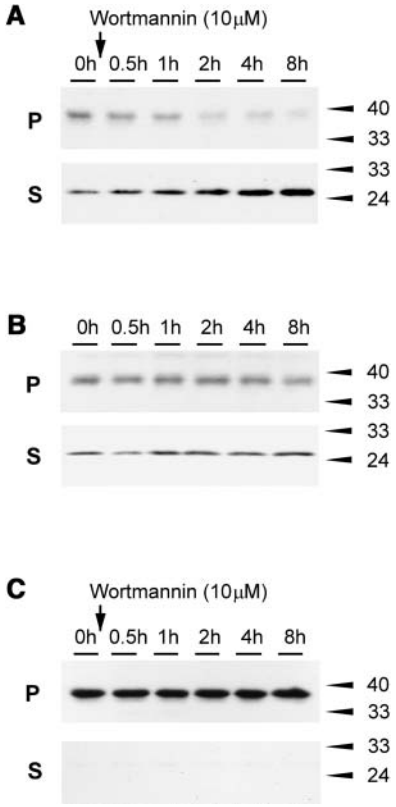

Figure 7. Wortmannin-Induced Degradation of GFP-BP80.

(A) Protoplasts were transfected with plasmid-encoding GFP-BP80a and incubated for 22 h, after which wortmannin was added for various time points. Membrane pellet (P) and soluble fractions (S; the sum of S1 and S2 in other figures) were analyzed by protein gel blots. Notice the increased level of the low molecular weight fragment (GFP core) and the decrease of the full-length fusion protein in function of time.

(B) The same conditions as in **(A)**, but the incubations were done without the drug. Notice that there is no change to the partitioning.

(C) Control experiment performed as in **(A)**, but where GFP-BP80a was replaced by GFP-CNX. Notice that no degradation fragment was detected and that the fusion protein did not diminish over time upon treatment with the drug.

GFP-spo and GFP-BP80a upon wortmannin treatment further, a pulse-chase analysis was performed. Unlike observing the change in cellular steady state levels, this technique allows us to measure protein traffic on de novo–synthesized cargo.

Figure 9 shows that the BP80-ligand GFP-spo chases rapidly into the soluble vacuolar GFP core fragment, with more than half of the precursor being converted into the lower molecular weight fragment after 8 h of chase (Figures 9A and 9B). Wortmannin drastically inhibits this transport as observed by a reduction of the chased vacuolar degradation product and a noticeable accumulation of full-length GFP-spo in the medium (Figure 9A, top panel). In contrast with the ligand, the receptor fusion protein chases much more slowly to the soluble vacuolar GFP core fragment, and after 8 h, only a small portion of the precursor has been degraded into the core fragment (compare left and right panels in Figure 9B).

Line scanning of phosphor imaging data and subsequent quantification via AIDA software (Raytest) revealed that after 8 h of chase, GFP-BP80–derived GFP core fragment levels were comparable to those derived from GFP-spo after just 2 h of chase (Figure 9C, compare the white bars). Likewise, the 1-h chase point for GFP-spo and the 4-h chase point for GFP-BP80 yielded a comparable percentage of GFP core fragments. Thus, the receptor construct is transported at an approximately fourfold lower rate compared with the ligand construct.

Most importantly, wortmannin treatment had completely opposite effects on ligand and receptor constructs. GFP-spo processing was slowed down, and GFP-BP80 processing was accelerated at all chase points (Figure 9C). Together with the results on the steady state levels (Figure 7), this result suggests that wortmannin inhibits the retrograde transport of GFP-BP80 between the PVC and the Golgi apparatus. For this reason, receptors are depleted from the Golgi apparatus leading to the secretion of their ligands.

DISCUSSION

Wortmannin Inhibits the BP80-Mediated Route to the Vacuole

We have shown that soluble cargo carrying a sequence-specific vacuolar sorting signal (amy-spo) is efficiently redirected to the cell surface by wortmannin in tobacco protoplasts and BY2 cells. This effect is seen over a broad concentration range and suggests that wortmannin interferes with the BP80-mediated transport to the vacuole. Amy-spo was confirmed as a BP80-ligand using soluble HDEL-tagged BP80 (sBP80-HDEL), a molecule that can inhibit vacuolar sorting via competition with the endogenous vacuolar sorting receptor (Watanabe et al., 2004). sBP80-HDEL coexpression resulted in a redistribution of amy-spo from the soluble vacuolar fraction to the microsomal fraction, but a mutant in which the vacuolar sorting signal was rendered nonfunctional by point mutation (Pimpl et al., 2003) was not affected. These results can only be explained by direct binding of amy-spo but not amy-spoM to the engineered BP80 molecule in vivo. Therefore, amy-spo can be considered a BP80-ligand.

During incubation with wortmannin, both full-length BP80 and sBP80-HDEL caused a meaningful reduction in the secretion of amy-spo but not amy, which provides further proof of the BP80 binding properties of amy-spo. More importantly, the experiments indicate that the drug does not inhibit ligand-receptor association directly. Although it is possible that conditions within the lumen of the secretory pathway change as a result of the drug, it did not prevent cell retention of amy-spo by overexpressed full-length BP80 or sBP80-HDEL (Figures 3A and 3C). Moreover, intracellular partitioning revealed that full-length BP80 overexpression retained amy-spo in the cells by restoring vacuolar sorting (Figure 3D).

Overexpressed full-length BP80a levels seem to be well above endogenous BP80 levels (Figure 3B) and can partially reverse the effect of wortmannin. It was this observation that initially led to our model in which the drug causes BP80 molecules to be

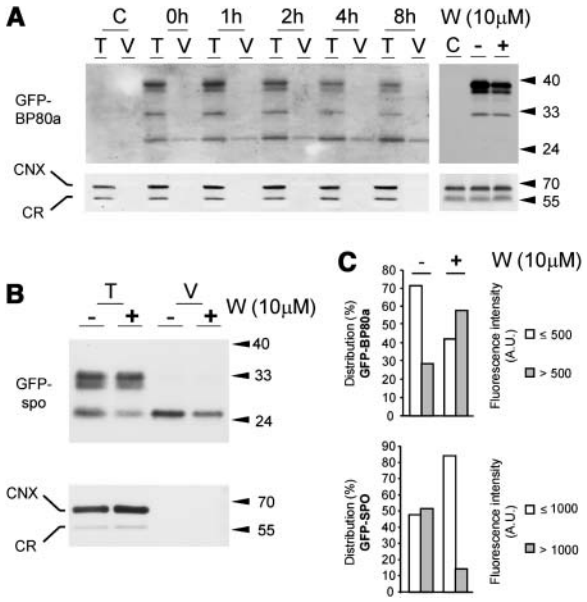

Figure 8. Vacuolar Localization of the Soluble GFP Core Fragment.

(A) After an initial incubation for 22 h to reach cellular steady state levels of transiently expressed GFP-BP80a, cells were incubated with 10 μM wortmannin for various times (indicated above each lane), after which total extracts (soluble + membrane proteins) from entire protoplasts (T) or purified vacuoles (V) isolated from the same protoplast suspensions were compared by protein gel blots. Equal levels of the vacuolar marker α-mannosidase were loaded to ensure a valid comparison. The left top panel was probed with anti-GFP serum, illustrating that wortmannin-induced increase in the soluble GFP core fragment is localized to the vacuoles. The panel at right is a similar protein gel blot but with microsomes purified from untransformed cells (C) and from cells transformed with GFP-BP80a. The latter were incubated for 22 h after which a further 4 h of incubation without (−) or with (+) wortmannin was performed. Notice the reduction of the full-length precursor in the wortmannin-treated sample, and the absence of the GFP core fragment from the microsomes in any sample. The bottom panels were probed with anticalnexin antibodies (Pimpl et al., 2000) that bind both ER markers calreticulin (CNX) and calnexin (CR). Notice that neither marker copurifies with the vacuoles and that all three microsomal fractions exhibit similar levels of these two ER markers.

(B) Vacuole partitioning assay as in **(A)** but with cells transfected with GFP-spo. Transfected cells were incubated for 22 h, after which a further 4 h of incubation without (−) or with (+) wortmannin was performed as in **(A)**. Notice the reduction of the GFP core fragment upon treatment with the drug both in total extracts (T) and in purified vacuoles (V).

(C) Quantification of the observed luminal green fluorescence of GFP-spo or GFP-BP80a derived GFP core fragments in vacuoles purified and analyzed by confocal laser scanning microscopy as shown in Figures 6C and 6D. One hundred fluorescent vacuoles were analyzed for either transfection, and fluorescence intensity is measured in arbitrary units (A.U.) using the same detector gains. To illustrate the effect of wortmannin, the population was split into two fractions (i.e., up to 500 A.U. and >500 A.U.). Because vacuolar fluorescence was higher in vacuoles purified in GFP-spo–transfected cells, we split the population differently (up to 1000 A.U. and above). Notice that the population of GFP-BP80a–containing vacuoles shifts from the low fluorescent class to the high class upon addition of the drug, whereas the opposite happens for GFP-spo-fluorescent vacuoles.

limiting, possibly by preventing retrograde transport of receptors from the PVC to the Golgi apparatus (see below).

Inhibition of Receptor Function through Competition

Although it is relatively easy to saturate the route taken by proteins carrying C-terminal vacuolar sorting signals (Neuhaus et al., 1994; Frigerio et al., 1998; Pimpl et al., 2003), it is not possible to saturate vacuolar sorting of cargo carrying an efficient sequence-specific vacuolar sorting signal, even in multicopy overexpression in transfected protoplasts (Pimpl et al., 2003). Unlike HDEL ligands that continuously recycle until the retention system fails (Phillipson et al., 2001), vacuolar proteins do not return from the lytic vacuole, and this may explain the lack of saturation. However, receptor molecules are limited to the membranes of the compartments in which they reside and have to be recycled from the compartment in which they have delivered their cargo. We postulated that sorting of BP80 would be easy to saturate because recycling receptors would join de novo–synthesized receptors. Limiting steps in the receptor recycling may then lead to missorting of ligands as well.

Therefore, we have created truncated-receptor molecules, in which the lumenal ligand binding domains were replaced by GFP (GFP-BP80). The transmembrane domains and cytosolic tails of Arabidopsis BP80 isoforms a, b, d, and f (Hadlington and Denecke, 2000; Paris and Neuhaus, 2002; Laval et al., 2003) were analyzed using this approach. Coexpression of all GFP-BP80 fusions strongly inhibited vacuolar sorting of the BP80-ligand amy-spo (shown for isoforms a and b in Figure 4) without affecting control ligands such as secreted amy or ER-retained amy-HDEL (Figure 5). This effect was dependent on the transmembrane domain and cytosolic tail of BP80 because the equivalent domains of calnexin did not show this effect.

The fusion protein is likely to compete with endogenous BP80 for its transport route (Figure 10). If GFP-BP80 occupies positions within the CCVs, this reduces the effectiveness of ligand transport because it excludes a portion of the endogenous BP80 pool from the vesicle. However, GFP-BP80 was mainly localized to extra-Golgi structures that are likely to represent the PVC (Figures 6A and 6B). This suggests that anterograde transport is not the limiting factor. If the clathrin-mediated anterograde route were limiting, GFP-BP80 should no longer arrive in a post-Golgi compartment and remain trapped in the Golgi. This was not the case, and even with drastic overproduction, only weak colocalization between GFP-BP80 and the Golgi marker was detected. This is not surprising because the vacuolar sorting receptor must also be present in the Golgi to retrieve its ligands. That its steady state levels are higher in the PVC suggests that retrograde rather than anterograde transport is limiting.

GFP-BP80 also reached a lytic compartment as shown previously with a similar truncated construct (Jiang and Rogers, 1998). This causes the appearance of a soluble GFP core fragment in the vacuoles, previously observed for secreted GFP, HDEL-tagged GFP, and GFP fused to vacuolar sorting signals (Frigerio et al., 2001; Brandizzi et al., 2003; Sohn et al., 2003). The GFP core fragment is a result of N-terminal and C-terminal processing of fused portions because the size is

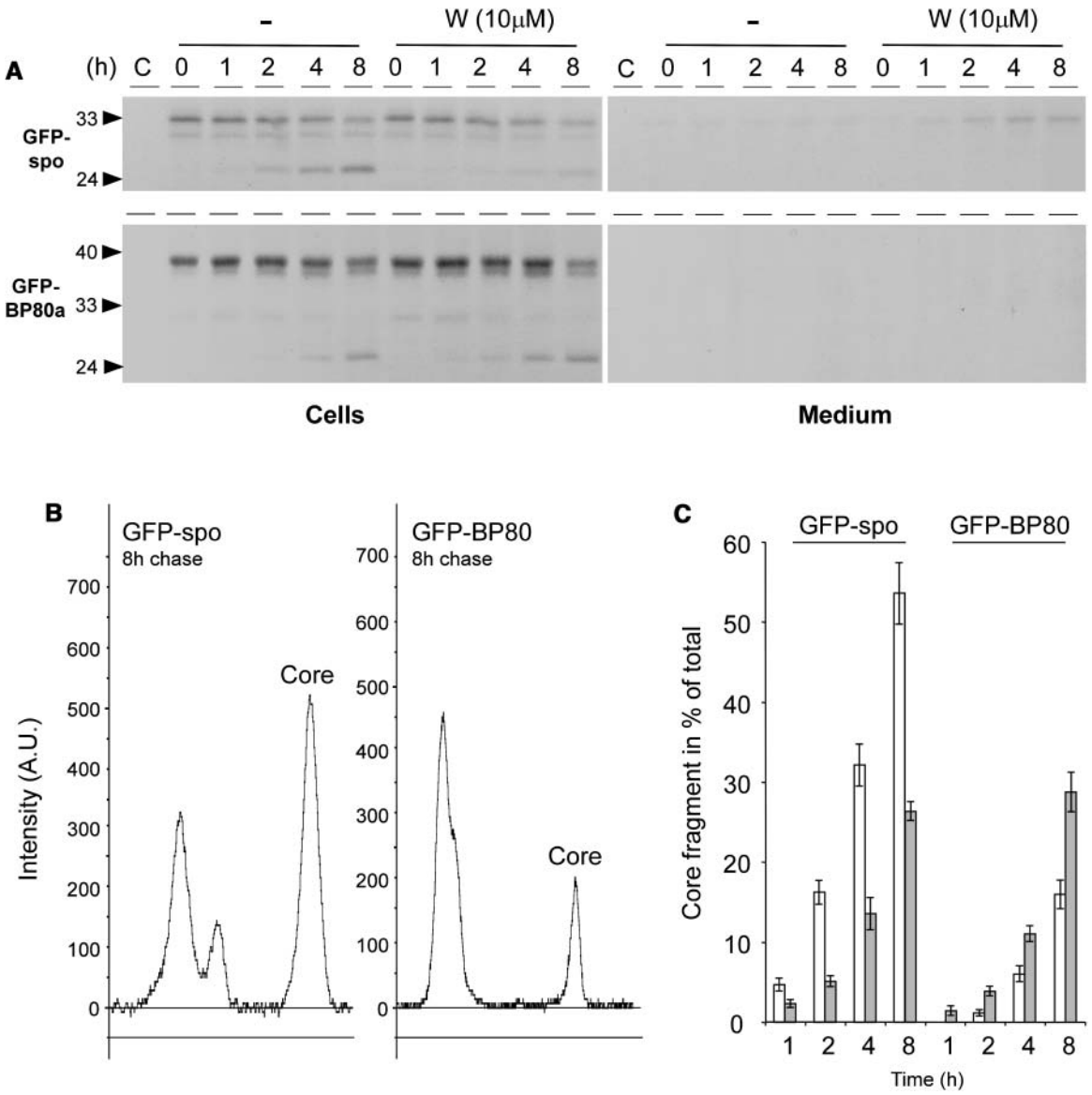

Figure 9. Pulse-Chase Analysis Demonstrating the Opposite Behavior of GFP-BP80a and GFP-spo in Response to the Drug Wortmannin.

(A) Protoplasts were pulse labeled for 1 h, after which incubation in chase buffer was conducted for times indicated above each lane either in the presence (W) or absence (–) of the drug wortmannin. Isolated medium and cell extracts were immunoprecipitated with the anti-GFP antiserum and separated by SDS-PAGE. Notice that both GFP-spo and GFP-BP80 chase into the GFP core fragment but that this is inhibited for GFP-spo upon incubation with wortmannin.

(B) Line scannings of the 8-h chase points for GFP-spo (left) and GFP-BP80a (right) from phosphor imaging data corresponding to **(A)** using AIDA software (Raytest). The signal for the GFP core fragment is indicated (Core) in each panel.

(C) GFP core fragment presented as a percentage of the total signal in each lane. Quantification of the GFP core signal bands was in arbitrary units and is presented as a percentage of the total surface area from all peaks in each lane. Percentages are given in function of the time for ligand (GFP-spo) and receptor construct (GFP-BP80) in the absence (white bars) and presence (gray bars) of 10 μM wortmannin. At the 1 h time point, GFP core was undetectable for GFP-BP80 in the absence of the drug.

independent of the various fused portions at either end of the molecule (Figure 4B; Brandizzi et al., 2003; S.L. Hanton, unpublished data). We could also demonstrate that the soluble GFP core fragment is not present in microsomes but purifies with vacuoles (Figure 8A). The observed leakage of GFP-BP80 to the vacuoles and degradation to the GFP core provides an argument to suggest that the truncated molecule saturates the recycling pathway from the PVC back to the Golgi. GFP-BP80 expression will drain the Golgi-PVC system of endogenous receptors that are then degraded in the vacuole (Figure 10B).

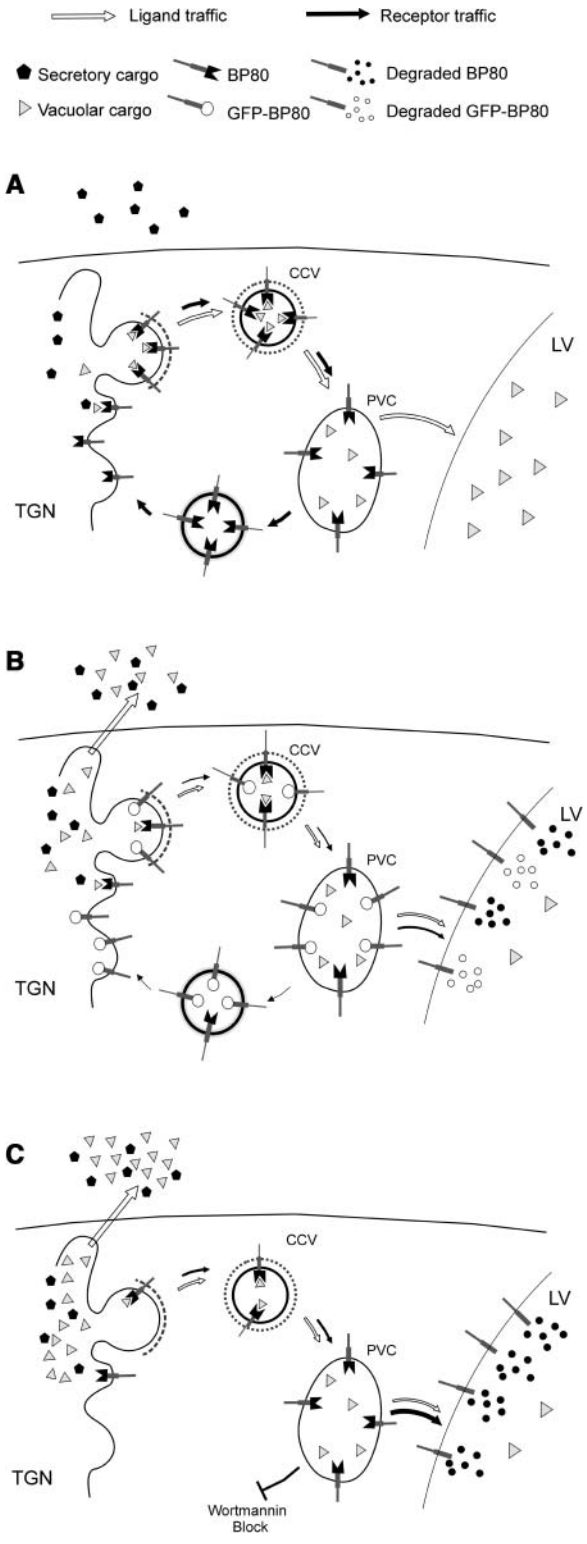

Figure 10. Model Explaining the Effects of Wortmannin and GFP-BP80 on Vacuolar Sorting.

Schematic representation of the Golgi-derived route to the PVC and the postulated retrograde route to recycle BP80 molecules.

The purpose of the suggested retrograde transport of vacuolar sorting receptors such as BP80 or the yeast VPS10 product from the PVC to the Golgi apparatus (Figure 10A) is to rescue them from degradation in the vacuoles (Pfeffer, 2001). This route is therefore as important as the anterograde route, and although the conditions favor ligand release in the PVC, this endosomal compartment should actively avoid proteolysis of the receptors. If the anterograde clathrin-mediated route were limiting during GFP-BP80 expression, additional synthesis of wild-type BP80 would cause further saturation rather than rescue. Instead, we have observed an efficient reconstitution of vacuolar sorting by an excess of full-length BP80. This illustrates that retrograde, rather than anterograde transport, is the limiting factor in the receptor traffic.

The semidominant behavior of truncated BP80 versus full-length BP80 is in sharp contrast with the effects observed with dominant negative mutants, where an excess of wild-type molecules did not effectively reconstitute the sorting process (Phillipson et al., 2001; Pimpl et al., 2003). Even 100-fold over-expression of the corresponding wild-type molecules could not prevent the dominant negative effect of ARF1(Q71L) or Sar1(H74L) (Phillipson et al., 2001; Pimpl et al., 2003).

Wortmannin Inhibits Efficient Receptor Recycling and Causes Leakage to the Vacuoles

In mammals, it has been shown that wortmannin disrupts the sorting of soluble lysosomal proteins (Davidson, 1995). Likewise, retrieval of the receptor Vps10p from the endosome in yeast is dependent on the activity of Vps34, a phosphatidylinositol 3-kinase (Stack and Emr, 1994; Seaman et al., 1997; Burda et al., 2002). Vps34 is essential for proper sorting of proteins to the endosome (Schu et al., 1993), and wortmannin is expected to inhibit this step. Therefore, it is tempting to postulate that wortmannin-induced depletion of BP80 could be because of an inhibition of the recycling of BP80 from the endosome (PVC) via a plant equivalent of the retromer-mediated pathway defined in *S. cerevisiae* (Seaman et al., 1997, 1998).

If BP80 cannot recycle back to the Golgi apparatus, it would be expected to reach the vacuole and suffer degradation (Figure

(A) Normal physiological situation. BP80 binds to ligands and mediates transport to the PVC via CCVs. Upon arrival in the PVC, the receptor releases the ligand and returns by means of a very efficient retrograde route back to the Golgi (black arrows). The BP80-ligands are then transported to the vacuole by default (white arrows).

(B) Truncated BP80 containing GFP instead of the ligand binding domain may compete with wild-type BP80 for entry into CCVs but also for recycling from the PVC. If sufficient GFP-BP80 is coexpressed, the retrograde route is saturated and leads to vacuolar deposition of GFP-BP80. This saturation also causes endogenous BP80 to be turned over in the vacuoles, giving rise to depleted BP80 numbers in the Golgi and reduced biosynthetic transport of receptors and ligands in the Golgi/PVC system (smaller arrows). BP80-ligands exhibit increased secretion to the medium (white arrow).

(C) Upon treatment with the drug wortmannin, BP80 is unable to return from the PVC to the Golgi and is degraded in the vacuole. This also leads to missorting of BP80-ligands to the cell surface.

10C), provided that recycling to the Golgi is the only mechanism to prevent loss of receptors to the vacuole. Wortmannin treatment of cells exhibiting steady state levels of GFP-BP80 in the PVC led to a very rapid redistribution of the fusion protein to the vacuolar lumen. Strong lumenal fluorescence was observed after just 2 h of incubation with wortmannin at the expense of punctate fluorescence in the PVC (Figures 6C and 6D). This effect was also observed biochemically via the wortmannin-induced increase in the vacuole-specific soluble GFP core fragment and a concomitant decrease of the full-length fusion protein (Figure 7).

Several controls were conducted to prove that wortmannin-induced soluble GFP core formation occurred in the vacuoles and was not because of differential effects of lumenal conditions such as the pH. Moreover, pulse-chase analysis confirmed the opposite behavior of GFP-spo and GFP-BP80 in response to the drug. The type I membrane-spanning GFP-BP80 fusion shows increased vacuolar sorting. By contrast, the vacuolar sorting of the soluble GFP-spo fusion is inhibited by the drug.

There are two strong arguments that suggest that wortmannin inhibits the retrograde transport of BP80. First of all, the drug caused further missorting of GFP-BP80 to the vacuole (Figures 6C, 6D, 7A, 8A, and 9A to 9C). Should wortmannin primarily inhibit the anterograde route, GFP-BP80 would have accumulated in the Golgi apparatus rather than leaking into the vacuole. If this were the case, formation of the soluble GFP core would be reduced. However, the opposite was observed. Secondly, overexpression of full-length BP80 could cause a partial rescue of vacuolar sorting (Figure 3). If wortmannin would inhibit vacuolar sorting via blocking the anterograde transport of BP80, overexpression of BP80 would not help at all. Because wortmannin does not affect the ER-Golgi route (Pimpl et al., 2003), overexpression of BP80 can replenish receptor levels at the Golgi apparatus even in the presence of the drug.

In contrast with the almost complete rescue of vacuolar sorting when competing with GFP-BP80 (Figure 5), wild-type BP80 expression only partially restores vacuolar sorting in the presence of wortmannin (Figure 3). This is possibly the result of a single usage of the receptors, which is inefficient compared with recycling. However, it is more likely that other molecules essential for Golgi-derived anterograde transport could be depleted by a lack of retrograde transport. Recycling of BP80 and membranes from the PVC will also retrieve soluble NSF attachment protein receptors (SNAREs) that are required for a new cycle of anterograde vesicle targeting. Rescue of vacuolar transport by coexpression of full-length BP80 alone will only proceed until the next factor will become limiting. Therefore, a range of components may have to be added to reconstitute wortmannin-inhibited vacuolar sorting completely. This highlights the need for well-defined biochemical experiments that can distinguish between primary effects and long-term effects of disrupting individual steps of the secretory pathway.

The model proposed in Figure 10C explains the existing data so far, but it will have to be refined once further elements of the recycling pathway between the PVC and the Golgi apparatus have been discovered. Likewise, the question regarding a possible involvement of early endosomes in vacuolar transport (Uemura et al., 2004) must be left unanswered until further research has been done.

METHODS

Plasmids for Transient Expression of Cargo Molecules

All DNA manipulations were done according to established procedures. The *Escherichia coli* MC1061 strain (Casadaban and Cohen, 1980) was used for the amplification of all plasmids. Previously established plasmids were used, encoding amy (Crofts et al., 1999), amy-HDEL (Phillipson et al., 2001), amy-spo, and amy-spoM (Pimpl et al., 2003). It was shown previously that the mutation of NPIRL to NPGRG in amy-spoM drastically increased the secretion of the fusion protein expected for a sequence-specific sorting signal (Pimpl et al., 2003). To further confirm the sequence-specific nature of the signal in amy-spo, we have also tested the effect of a double-Gly to the C terminus (amy-spoGG). This construct was generated by inserting annealed oligonucleotide pairs between the *Bgl*II and *Xba*I sites of the amy encoding plasmid that overlap with the last codon and the stop codon as described previously (Pimpl et al., 2003). The following oligonucleotide pairs were used to generate the C-terminally fused peptide encoding regions: spoGG-sense (5′-GATCA-GATTCAATCCCATCCGCCTCCCCACCACACACGGTGGATAAT-3′) and spoGG antisense (5′-CTAGATTATCCACCGTGTGTGGTGGGGAGGCG-GATGGGATTGAATCT-3′). Underlined areas represent the additional double codons for the double glycin motif added at the C terminus of the sporamin-sorting signal. The new construct was verified by sequencing analysis. As expected, this extended fusion exhibited properties indistinguishable from those reported for amy-spo (data not shown).

ST-YFP in pLL4 was created by amplification of the ST-YFP sequence from pVKH18En6::ST-YFP described earlier (Brandizzi et al., 2002) using a forward primer (5′-GGCCGCATGGATGATTCATACCAACTTGAAGA-AAAAGTTCAGCCTCTTCATCCTGG-3′) and a reverse primer (5′-GCG-CCGGGATCCTTACAAATCCTCCTCAGAGATAAGTTTCTGC-3′) using *Cla*I and *Bam*HI restriction sites in pLL4 (Brandizzi et al., 2003).

A glycosylated-GFP variant was recreated from published instructions (Batoko et al., 2000) but with the following modifications: instead of the chitinase signal peptide, the signal peptide of sweet potato (*Ipomoea batatas*) sporamin was used, amplified with the oligos FB35 (5′-GCGCGAATCGATGAAAGCCTTCACACTCGCTCTCTTCTTA-3′) and FB100 (5′-GTGCCGCAGGTGAGTCGACGTCATGGCTGGATTGGGC-AGGAGATAGAGGG-3′), cut with *Cla*I and *Sal*I, for insertion into pLL4 (Brandizzi et al., 2003). The *Cla*I site gives rise to the fusion with pCaMV35S, and *Sal*I provides the link with the glycosylation peptide that was recreated using two oligonucleotides composing the published sequence (Batoko et al., 2000). Secondly, a *Bgl*II site was engineered at the C terminus of the modified GFP to permit C-terminal extensions between *Bgl*II and *Xba*I, the latter of which overlaps with the stop codon (Brandizzi et al., 2003). This was accomplished with the oligo GFP-*Bgl*II (5′-TCTTGCAGATCTCGGATCCTTCTGCTCCTTTGTA-3′) that was used in conjunction with FB35 to amplify the entire coding region of the *N*-glycosylated variant of GFP. The vacuolar cargo molecule GFP-spo was synthesized with the same oligonucleotides as described for amy-spo (Pimpl et al., 2003).

Plasmids for Transient Expression of Effector Molecules

The transmembrane domain and cytosolic tail of *Arabidopsis thaliana* Calnexin was amplified using sense oligo 5′-ACCGAGATCTCGGAACT-GATTGAGAAAGCC-3′ and antisense oligo 5′-ATCCTCTAGAGCTAAT-TATCACGTCTCG-3′ from first-strand cDNA prepared from 3-d-old seedlings of Arabidopsis according to established procedures (Pimpl et al., 2003). The underlined regions refer to engineered restriction sites for insertion between *Bgl*II and *Xba*I for insertion between the coding region of the *N*-glycosylated variant of GFP and its stop codon to create a C-terminal fusion, yielding the plasmid pSLH6.

The transmembrane domain and cytoplasmic tail of the BP80 were amplified by PCR from first-strand cDNA prepared from 3-d-old seedlings of Arabidopsis, using the following oligonucleotide pairs: BP80a-sense (5′-TCCAAGACGGGTTCACAAGTG-3′) and BP80a-antisense (5′-CCATTTGGATCCCTTAGGCACGTTCATCATTC-3′); BP80b-sense (5′-TGTTCAGGCAAAGTTGGAACC-3′) and BP80b-antisense (5′-ACTTCATCTAGATATCCATATGGTGACCACT-3′); BP80d-sense (5′-ACAAGAGATCTCTATTGAGAGAAGCGGATCAAG-3′) and BP80d-antisense (5′-CAAGATTTTCTAGATTAGGCTGCAGAAGTTAATC-3′); BP80f-sense (5′-TCAAGAGATCTCTATAGAGAGATATGGATCCAAACG-3′) and BP80f-antisense (5′-ATACTTCTAGAGTGTAAAAGGCTCGGC-3′). The BP80a PCR amplification product was digested with *Bam*HI, the BP80b fragment with *Xba*I, and BP80d and BP80f were digested with both *Bgl*II and *Xba*I for vector insertion.

The fragment encoding the 35S promoter and GFP fused to the signal peptide of sweet potato sporamin was extracted from the plasmid pSLH6 by digestion with *Bgl*II, filling in by using the Klenow fragment, and digestion with *Eco*RI. This fragment and the digested BP80a fragment were gel purified and inserted into pLL4 (Brandizzi et al., 2003), previously cut with *Eco*RI/*Bam*HI, and dephosphorylated with calf intestine phosphatase. This resulted in fusion of the truncated BP80a downstream and in frame with the GFP sequence, yielding the plasmid pLL38. GFP-BP80b was constructed similarly, except for the use of *Xba*I before the 3′nos sequence in pLL4 and yielded pLL40. GFP-BP80d and GFP-BP80f were constructed by replacing the calnexin transmembrane domain and cytosolic tail of pSLH6 by straightforward swapping of the *Bgl*II-*Xba*I fragment with the amplified and digested BP80d and BP80f fragments, yielding pFox1 and pFox2.

Full-length BP80a (Hadlington and Denecke, 2000) was amplified from the same cDNA using the oligos BP80aFL-sense (5′-AAGCAGCTTCTGTGTTATCTT-3′) and BP80a-antisense (described above) and cloned in pAmy (Crofts et al., 1999) between the blunted *Nco*I site and the sticky *Bam*HI site, effectively replacing the amy coding region by the full-length coding region of BP80a, yielding plasmid pJLH21. Soluble BP80a fragments with and without HDEL motifs and supplemented by C-terminal Myc tags were constructed in the same way, except that the following antisense oligonucleotide was used: 5′-CCTAGCTAGCTAGCCAGGTCCTCCTCGGAGATCAGCTTCTGCTCCATCGTCTTGCTGATGCAAGTGTC-3′. The PCR fragment was cut with *Nhe*I and cloned between blunted *Nco*I and sticky *Nhe*I in pDE800 (containing C-terminal HDEL) or pDE801 (Leborgne-Castel et al., 1999), yielding pJLH20 and pJLH19. All constructions were verified by sequencing analysis.

Transient Expression and Plant Material

Tobacco plants (*Nicotiana tabacum* cv Petit Havana) (Maliga et al., 1973) were grown in MS medium (Murashige and Skoog, 1962) and 2% sucrose in a controlled room at 25°C with a 16-h day length at the light irradiance of 200 $\mu E/m^2/s$. Preparation of tobacco leaf protoplasts and transfection via electroporation were done as described previously (Phillipson et al., 2001), and plasmid concentrations used are given in the figure legends. All incubations were performed for 24 h unless otherwise indicated. The harvesting of cells and culture medium was described previously (Phillipson et al., 2001; Törmäkangas et al., 2001; Pimpl et al., 2003).

Drug Incubations

Wortmannin was dissolved as a 33 mM stock solution in DMSO and subsequently diluted in transient expression (TEX) buffer (Phillipson et al., 2001) as appropriate. The final concentration and incubation time in the presence of the drug are as described in Results and in the figure legends. To ensure constant background parameters for drug dosage experiments, a slightly modified electroporation protocol was used. Six hundred–microliter batches of electroporated-protoplast suspensions (containing 2.5×10^6 cells) were initially diluted with 1000 μL of TEX medium and then pooled. The protoplasts were then split into equal portions of 1000 μL and supplemented with another 1000 μL of TEX medium that contains twice the final concentration of the drug indicated in the figure legends. This ensured minimal variation between the samples except for the concentration of the drug. Individual samples were then harvested as described previously (Phillipson et al., 2001).

Vacuole Preparation and Cell Partitioning by Osmotic Shock

Vacuoles were isolated from protoplasts 24 h after electroporation in transient expression experiments as described (Törmäkangas et al., 2001), except for the following modifications: the cellulose synthesis inhibitor, 2,6-dichlorobenzonitrile, was omitted as it proved unnecessary. Moreover, both the pelleted vacuoles and the total protoplast pellet were resuspended in 100 μL of vacuole buffer (Törmäkangas et al., 2001), of which 50 μL were immediately frozen after mixing with 50 μL of SDS sample buffer. An identical aliquot of 50 μL was diluted with 100 μL of α-mannosidase extraction buffer (Törmäkangas et al., 2001), sonicated, and spun for 5 min in a refrigerated Eppendorf centrifuge to yield a clear supernatant for α-mannosidase assays. The total and vacuole samples for SDS-PAGE were adjusted to the appropriate dilution via obtained marker values using a 50/50 vacuole buffer/SDS sample buffer mix. Equal α-mannosidase levels for cells and vacuoles were then loaded on SDS gels for further analysis.

Cell partitioning through osmotic shock treatment was performed using an established procedure (Denecke et al., 1992) except that amy extraction buffer was used. Cells pelleted with 250 mM NaCl were gently resuspended in a fourfold volume of amy extraction buffer and incubated on ice for 5 min. Centrifugation of the samples at 25,000*g* for 15 min yields osmotically released soluble proteins in the supernatant (termed fraction S1) that are mainly cytoplasmic and vacuolar, whereas microsomes formed the pellet. The pellet was resuspended in the same volume of amy extraction buffer as S1, sonicated, and pelleted at 25,000*g* for 15 min. This yields all remaining soluble microsomal proteins and some membrane proteins (termed fraction S2). The resulting pellet (P) is highly enriched in membranes and was resuspended in the same volume of amy extraction buffer as S1 or S2, sonicated, and left in suspension until analyzed by SDS-PAGE.

Enzymatic Assays

For standard amy assays, the cells were extracted in amy extraction buffer (Crofts et al., 1999) via sonication for 5 s. This corresponds to the combined S1 and S2 fractions described in the previous paragraph. The extracts were centrifuged for 10 min at 25,000*g* at 4°C, and the clean soluble supernatant was recovered. The culture medium was also spun for 10 min at 25,000*g* at 4°C to remove residual cell debris. The amy assays and calculation of the secretion index as the ratio between the extracellular and intracellular activity were described previously (Denecke et al., 1990; Crofts et al., 1999; Phillipson et al., 2001; Pimpl et al., 2003). In Figure 5C, soluble amy-extract (S) and pellet (P) were used for protein gel blotting (see below) to assess the level of effector molecule in the BP80 rescue experiment.

The α-mannosidase assays for vacuolar partioning experiments were performed as described previously (Törmäkangas et al., 2001; Pimpl et al., 2003). The amount of α-mannosidase activity was used to equalize the loading of cells and purified vacuoles on SDS-polyacrylamide gels. The levels of calnexin were analyzed by protein gel blots as a control for ER contamination in the vacuole preparations.

Protein Extraction and Gel Blot Analysis

Protein analysis of culture medium was performed after concentration with aqueous ammonium sulfate solution (60% final) for 2 h on ice, using

BSA at 0.5 mg/mL as a carrier. The protein precipitate was obtained by 10-min centrifugation at 4°C in a refrigerated Eppendorf centrifuge at maximum speed, then resuspended in amy extraction buffer to obtain a 10-fold higher concentration compared with the original volume of cell suspension. Cellular proteins were analyzed separately as soluble proteins and membrane proteins. The cell pellet was resuspended in a 10-fold lower volume of amy extraction buffer, and soluble cell proteins were extracted by sonication and centrifugation for 10 min at 25,000*g* at 4°C. The supernatant containing the soluble proteins was recovered. The pellet containing membrane proteins was resuspended in an equal volume of amy extraction buffer followed by brief sonication to obtain a homogeneous solution (membrane-enriched fraction).

Protein cell extracts enriched in soluble (S1, S2, or combined S1/S2) or membrane proteins (P) as well as the concentrated medium were loaded in equal volumes after twofold dilution with 2× SDS loading buffer (Crofts et al., 1999) and brief boiling (5 min, 95°C). Proteins in SDS-polyacrylamide gels were transferred onto a nitrocellulose membrane and then blocked with PBS, 05% Tween 20, and 5% milk powder for 1 h.

After gel blotting, immunodetections were performed using enhanced chemiluminescence, using rabbit polyclonal antiserum raised against GFP (1:5000 dilution), BP80 (1:10,000) (Laval et al., 1999), or calnexin (1:15,000) (Pimpl et al., 2000).

Purification of Anti-BP80 Antiserum (640SF) by Subtraction

The polyclonal antiserum 640SF (Laval et al., 1999) prepared against a conserved BP80 domain proved to contain high background staining of our protein gel blots. To reduce the background, 5 g of tobacco plants were extracted with 5 mL of 50 mM Tris, 1 mM EDTA with mortar and pestle and spun for 5 min at 20,000*g* to remove debris and then 1 h at 100,000*g* to remove membranes. The supernatant was diluted to 50 mL with PBS and incubated with 20 cm^2 of nitrocellulose membrane for 1 h. These membranes were then blocked with milk, washed with PBS-Tween, and then used as solid-state subtractor for incubation with 50 mL of 1000-fold diluted serum in 1× PBS supplemented with 1% BSA, 0.02% sodium azide. After overnight incubation, the diluted and subtracted antibody was kept at 4°C and used for routine protein gel blots.

Preparation of Microsomes from Transfected Protoplasts

To detect transiently expressed BP80 in tobacco protoplasts, it was necessary to prepare microsomes (Laval et al., 1999). Microsomes were also prepared to rule out the presence of the soluble GFP core fragment in this fraction. Protoplasts from five batches of transfections were pooled and incubated for 24 h, after which cells were separated from the medium and debris via floatation in TEX medium. After removing the majority of underlying solution, floating cells were washed in 50 mL of 250 mM NaCl and pelleted. The pellets were resuspended in 3 mL homogenization buffer (50 mM Tris-HCl, pH 8.0, 1 mM $CaCL_2$, 1 g/L polyvinylpyrrolidone, 1 μg/mL pepstatin, 10 mM ascorbic acid, and 2 mM sodium metabisulfite) supplemented with 12% (w/w) of sucrose, passed through a syringe needle five times, and then centrifuged for 10 min at 2000*g* in a swing-out rotor. Two milliliters of turbid supernatant was carefully layered onto a 9-mL 20% sucrose cushion (in homogenization buffer) and centrifuged through the cushion onto a second 55% sucrose cushion (in homogenization buffer) by ultracentrifugation (35,000 rpm, SW41 swing-out rotor, 1.5 h, and 4°C). Microsomes were collected in 250 μL from the 20 to 55% interface and mixed with 250 μL of SDS-PAGE sample buffer and boiled and separated by SDS-PAGE. BP80, GFP-BP80, or calnexin was monitored by protein gel blots.

Confocal Laser Scanning Microscopy

Protoplasts expressing the GFP and YFP fusions were harvested 24 h after DNA transfer and embedded in 1% low melting agarose in TEX medium on a slide to prevent vibrations. Confocal imaging was performed using an inverted Zeiss LSM 510 META laser scanning microscope (Zeiss, Jena, Germany) with a Plan-Neofluar 40×/1.3 oil differential interference contrast objective. For imaging expression of either GFP constructs alone or in combination with ST-YFP, excitation lines of an argon laser of 458 nm for GFP and 514 nm for YFP were used alternately with line switching using the multitrack facility of the microscope. The fluorescence was detected using a 458/514 dichroic beam splitter and 475- to 525-nm band-pass filter for GFP and 560- to 615-nm band pass filter for YFP. Appropriate controls have been performed to exclude the possibility of cross talk between the two fluorochromes before the experiments. Postacquisition image processing was with the LSM 5 image browser (Zeiss) and Adobe Photoshop Elements software (Mountain View, CA). To quantify GFP fluorescence with arbitrary units, identical detector gains were used for all measurements.

In Vivo Labeling and Immunoprecipitation

For pulse-chase analysis of GFP-spo and GFP-BP80, 10 standard electroporations were pooled, washed, and concentrated in 500 μL of TEX buffer supplemented with 100 μCi/mL Pro-mix (Amersham Life Sciences, Buckinghamshire, UK). After pulse labeling for 1 h, protoplasts were diluted with chase buffer (10 mM Met and 5 mM Cys in TEX buffer) in the presence or absence of wortmannin (10 μM final concentration). The protoplast suspensions were split into equal portions and incubated at 25°C for an appropriate period of time (as stated in the figure legends). Medium and cells were harvested as described above. The immunoprecipitations were performed on ice using ice-cold buffers. The cellular fractions were extracted in homogenization buffer (200 mM Tris-HCl, pH 8.0, 300 mM NaCl, 1% Triton X-100, and 1 mM EDTA). The homogenate was centrifuged for 5 min at 4°C in an Eppendorf-refrigerated centrifuge. The supernatant was isolated and stored at −80°C. Culture medium was frozen immediately after harvesting. Media and cell extracts were precipitated in NET gel buffer (50 mM Tris-HCl, pH 7.5, 150 mM NaCl, 1 mM EDTA, 0.1% IGEPAL CA-630, 0.02% NaN_3, and supplemented with 0.25% gelatin), containing anti-GFP antiserum (Molecular Probes, Eugene, OR; 1/1000 dilution). After 1-h incubation on ice and centrifugation to remove aggregates, the supernatant was transferred to another Eppendendorf tube containing 2.5 mg of hydrated Protein A-Sepharose (Sigma-Aldrich, St. Louis, MO) in NET buffer. The samples were incubated for 2 h at 4°C with slow rotation. Protein A-Sepharose was then pelleted by centrifugation for 10 s at 5000*g*, and the supernatant was discarded. The pellet was washed four times with NET buffer and a fifth wash with PBS. Thirty microliters of SDS-PAGE sample buffer were added to the final pellet, and the suspension was incubated at 95°C for 5 min and analyzed by SDS-PAGE. Labeled proteins were detected by phosphor imaging (Fuji Film FLA 500; Tokyo, Japan) and AIDA software (Raytest; Raytek Scientific, Sheffield, UK) to allow quantification. Exposures on x-ray films were used to obtain higher resolution images for visual display (Figure 9A). The percentage of processing was determined for each lane by dividing the peak surface area of the GFP core band by the total surface area of all peaks (Figure 9C) and multiplication by 100 to yield percentages.

ACKNOWLEDGMENTS

This work was supported by grants from the Biotechnology and Biological Sciences Research Council and the European Union (HPRN-CT-2002-00262: BioInteractions). J. Galaud (Université Paul Sabatier, France) is thanked for the generous gift of the antiserum 640SF directed against a conserved epitope of AtBP80. L.L.P.d.S. is indebted to CAPES-Brazilian Government for a PhD studentship. J.L.H., S.L.H.,

C.J.S., and O.F. are indebted to the Biotechnology and Biological Sciences Research Council for their PhD studentships. Gareth Howell is thanked for help with the BioImaging facility at Leeds, and funding from the Wellcome Trust (reference no. 065321) and the Science Research Investment Fund of the UK Higher Education Funding Council for England is gratefully acknowledged. P. Pimpl is thanked for critically reading the manuscript and advice with the microsomal membrane preparations. S.J.F. wishes to thank her fellow third year project students Olivia Alder and Styliani Tsiapou for stimulating discussions.

Received July 26, 2004; accepted October 8, 2004.

REFERENCES

Ahmed, S.U., Bar-Peled, M., and Raikhel, N.V. (1997). Cloning and subcellular location of an Arabidopsis receptor-like protein that shares common features with protein-sorting receptors of eukaryotic cells. Plant Physiol. **114,** 325–336.

Ahmed, S.U., Rojo, E., Kovaleva, V., Venkataraman, S., Dombrowski, J.E., Matsuoka, K., and Raikhel, N.V. (2000). The plant vacuolar sorting receptor AtELP is involved in transport of NH(2)-terminal propeptide-containing vacuolar proteins in *Arabidopsis thaliana*. J. Cell Biol. **149,** 1335–1344.

Bassham, D.C., and Raikhel, N.V. (2000). Unique features of the plant vacuolar sorting machinery. Curr. Opin. Cell Biol. **12,** 491–495.

Batoko, H., Zheng, H.Q., Hawes, C., and Moore, I. (2000). A rab1 GTPase is required for transport between the endoplasmic reticulum and Golgi apparatus and for normal Golgi movement in plants. Plant Cell **12,** 2201–2218.

Brandizzi, F., Frangne, N., Marc-Martin, S., Hawes, C., Neuhaus, J.M., and Paris, N. (2002). The destination for single-pass membrane proteins is influenced markedly by the length of the hydrophobic domain. Plant Cell **14,** 1077–1092.

Brandizzi, F., Hanton, S., DaSilva, L.L., Boevink, P., Evans, D., Oparka, K., Denecke, J., and Hawes, C. (2003). ER quality control can lead to retrograde transport from the ER lumen to the cytosol and the nucleoplasm in plants. Plant J. **34,** 269–281.

Burda, P., Padilla, S.M., Sarkar, S., and Emr, S.D. (2002). Retromer function in endosome-to-Golgi retrograde transport is regulated by the yeast Vps34 PtdIns 3-kinase. J. Cell Sci. **115,** 3889–3900.

Casadaban, M.J., and Cohen, S.N. (1980). Analysis of gene control signals by DNA fusion and cloning in *Escherichia coli*. J. Mol. Biol. **138,** 179–207.

Chrispeels, M.J. (1983). The Golgi-apparatus mediates the transport of phytohemagglutinin to the protein bodies in bean cotyledons. Planta **158,** 140–151.

Crofts, A.J., Leborgne-Castel, N., Hillmer, S., Robinson, D.G., Phillipson, B., Carlsson, L.E., Ashford, D.A., and Denecke, J. (1999). Saturation of the endoplasmic reticulum retention machinery reveals anterograde bulk flow. Plant Cell **11,** 2233–2248.

Davidson, H.W. (1995). Wortmannin causes mistargeting of procathepsin D. Evidence for the involvement of a phosphatidylinositol 3-kinase in vesicular transport to lysosomes. J. Cell Biol. **130,** 797–805.

Denecke, J., Botterman, J., and Deblaere, R. (1990). Protein secretion in plant cells can occur via a default pathway. Plant Cell **2,** 51–59.

Denecke, J., De Rycke, R., and Botterman, J. (1992). Plant and mammalian sorting signals for protein retention in the endoplasmic reticulum contain a conserved epitope. EMBO J. **11,** 2345–2355.

Frigerio, L., de Virgilio, M., Prada, A., Faoro, F., and Vitale, A. (1998). Sorting of phaseolin to the vacuole is saturable and requires a short C-terminal peptide. Plant Cell **10,** 1031–1042.

Frigerio, L., Foresti, O., Felipe, D.H., Neuhaus, J.M., and Vitale, A. (2001). The C-terminal tetrapeptide of phaseolin is sufficient to target green fluorescent protein to the vacuole. J. Plant Physiol. **158,** 499–503.

Hadlington, J.L., and Denecke, J. (2000). Sorting of soluble proteins in the secretory pathway of plants. Curr. Opin. Plant Biol. **3,** 461–468.

Hara-Nishimura, I., Shimada, T., Hatano, K., Takeuchi, Y., and Nishimura, M. (1998). Transport of storage proteins to protein storage vacuoles is mediated by large precursor-accumulating vesicles. Plant Cell **10,** 825–836.

Hillmer, S., Movafeghi, A., Robinson, D.G., and Hinz, G. (2001). Vacuolar storage proteins are sorted in the cis-cisternae of the pea cotyledon Golgi apparatus. J. Cell Biol. **152,** 41–50.

Hinz, G., Hillmer, S., Baumer, M., and Hohl, I. (1999). Vacuolar storage proteins and the putative vacuolar sorting receptor BP-80 exit the Golgi apparatus of developing pea cotyledons in different transport vesicles. Plant Cell **11,** 1509–1524.

Hoh, B., Hinz, G., Jeong, B.K., and Robinson, D.G. (1995). Protein storage vacuoles form de novo during pea cotyledon development. J. Cell Sci. **108,** 299–310.

Hohl, I., Robinson, D.G., Chrispeels, M.J., and Hinz, G. (1996). Transport of storage proteins to the vacuole is mediated by vesicles without a clathrin coat. J. Cell Sci. **109,** 2539–2550.

Humair, D., Hernandez Felipe, D., Neuhaus, J.M., and Paris, N. (2001). Demonstration in yeast of the function of BP-80, a putative plant vacuolar sorting receptor. Plant Cell **13,** 781–792.

Jiang, L., and Rogers, J.C. (1998). Integral membrane protein sorting to vacuoles in plant cells: Evidence for two pathways. J. Cell Biol. **143,** 1183–1199.

Kim, D.H., Eu, Y.J., Yoo, C.M., Kim, Y.W., Pih, K.T., Jin, J.B., Kim, S.J., Stenmark, H., and Hwang, I.I. (2001). Trafficking of phosphatidylinositol 3-phosphate from the trans-Golgi network to the lumen of the central vacuole in plant cells. Plant Cell **13,** 287–301.

Kirsch, T., Paris, N., Butler, J.M., Beevers, L., and Rogers, J.C. (1994). Purification and initial characterization of a potential plant vacuolar targeting receptor. Proc. Natl. Acad. Sci. USA **91,** 3403–3407.

Kirsch, T., Saalbach, G., Raikhel, N.V., and Beevers, L. (1996). Interaction of a potential vacuolar targeting receptor with amino- and carboxyl-terminal targeting determinants. Plant Physiol. **111,** 469–474.

Laval, V., Chabannes, M., Carriere, M., Canut, H., Barre, A., Rouge, P., Pont-Lezica, R., and Galaud, J. (1999). A family of Arabidopsis plasma membrane receptors presenting animal beta-integrin domains. Biochim. Biophys. Acta **1435,** 61–70.

Laval, V., Masclaux, F., Serin, A., Carriere, M., Roldan, C., Devic, M., Pont-Lezica, R.F., and Galaud, J.P. (2003). Seed germination is blocked in Arabidopsis putative vacuolar sorting receptor (atbp80) antisense transformants. J. Exp. Bot. **54,** 213–221.

Leborgne-Castel, N., Jelitto-Van Dooren, E.P., Crofts, A.J., and Denecke, J. (1999). Overexpression of BiP in tobacco alleviates endoplasmic reticulum stress. Plant Cell **11,** 459–470.

Levanony, H., Rubin, R., Altschuler, Y., and Galili, G. (1992). Evidence for a novel route of wheat storage proteins to vacuoles. J. Cell Biol. **119,** 1117–1128.

Li, Y.B., Rogers, S.W., Tse, Y.C., Lo, S.W., Sun, S.S., Jauh, G.Y., and Jiang, L. (2002). BP-80 and homologs are concentrated on post-Golgi. Probable lytic prevacuolar compartments. Plant Cell Physiol. **43,** 726–742.

Maliga, P., Sz-Breznovits, A., and Marton, L. (1973). Streptomycin-resistant plants from callus culture of haploid tobacco. Nat. New. Biol. **244,** 29–30.

Marcusson, E.G., Horazdovsky, B.F., Cereghino, J.L., Gharakhanian, E., and Emr, S.D. (1994). The sorting receptor for yeast vacuolar carboxypeptidase Y is encoded by the VPS10 gene. Cell **77,** 579–586.

Matsuoka, K., Bassham, D.C., Raikhel, N.V., and Nakamura, K. (1995). Different sensitivity to wortmannin of two vacuolar sorting signals indicates the presence of distinct sorting machineries in tobacco cells. J. Cell Biol. **130,** 1307–1318.

Miller, E.A., Lee, M.C., and Anderson, M.A. (1999). Identification and characterization of a prevacuolar compartment in stigmas of *Nicotiana alata*. Plant Cell **11,** 1499–1508.

Murashige, R., and Skoog, F. (1962). A revised medium for rapid growth and bioassays with tobacco tissue cultures. Physiol. Plant. **15,** 473–497.

Neuhaus, J.M., Pietrzak, M., and Boller, T. (1994). Mutation analysis of the C-terminal vacuolar targeting peptide of tobacco chitinase: Low specificity of the sorting system, and gradual transition between intracellular retention and secretion into the extracellular space. Plant J. **5,** 45–54.

Palade, G. (1975). Intracellular aspects of the process of protein synthesis. Science **189,** 347–358.

Paris, N., and Neuhaus, J.M. (2002). BP-80 as a vacuolar sorting receptor. Plant Mol. Biol. **50,** 903–914.

Paris, N., Rogers, S.W., Jiang, L., Kirsch, T., Beevers, L., Phillips, T.E., and Rogers, J.C. (1997). Molecular cloning and further characterization of a probable plant vacuolar sorting receptor. Plant Physiol. **115,** 29–39.

Paris, N., Stanley, C.M., Jones, R.L., and Rogers, J.C. (1996). Plant cells contain two functionally distinct vacuolar compartments. Cell **85,** 563–572.

Pfeffer, S.R. (2001). Membrane transport: Retromer to the rescue. Curr. Biol. **11,** R109–R111.

Phillipson, B.A., Pimpl, P., daSilva, L.L., Crofts, A.J., Taylor, J.P., Movafeghi, A., Robinson, D.G., and Denecke, J. (2001). Secretory bulk flow of soluble proteins is COPII dependent. Plant Cell **13,** 2005–2020.

Pimpl, P., Hanton, S.L., Taylor, J.P., Pinto-daSilva, L.L., and Denecke, J. (2003). The GTPase ARF1p controls the sequence-specific vacuolar sorting route to the lytic vacuole. Plant Cell **15,** 1242–1256.

Pimpl, P., Movafeghi, A., Coughlan, S., Denecke, J., Hillmer, S., and Robinson, D.G. (2000). In situ localization and in vitro induction of plant COPI-coated vesicles. Plant Cell **12,** 2219–2236.

Sanderfoot, A.A., Ahmed, S.U., Marty-Mazars, D., Rapoport, I., Kirchhausen, T., Marty, F., and Raikhel, N.V. (1998). A putative vacuolar cargo receptor partially colocalizes with AtPEP12p on a prevacuolar compartment in Arabidopsis roots. Proc. Natl. Acad. Sci. USA **95,** 9920–9925.

Schu, P.V., Takegawa, K., Fry, M.J., Stack, J.H., Waterfield, M.D., and Emr, S.D. (1993). Phosphatidylinositol 3-kinase encoded by yeast VPS34 gene essential for protein sorting. Science **260,** 88–91.

Seaman, M.N., Marcusson, E.G., Cereghino, J.L., and Emr, S.D. (1997). Endosome to Golgi retrieval of the vacuolar protein sorting receptor, Vps10p, requires the function of the VPS29, VPS30, and VPS35 gene products. J. Cell Biol. **137,** 79–92.

Seaman, M.N., McCaffery, J.M., and Emr, S.D. (1998). A membrane coat complex essential for endosome-to-Golgi retrograde transport in yeast. J. Cell Biol. **142,** 665–681.

Shimada, T., Fuji, K., Tamura, K., Kondo, M., Nishimura, M., and Hara-Nishimura, I. (2003). Vacuolar sorting receptor for seed storage proteins in *Arabidopsis thaliana*. Proc. Natl. Acad. Sci. USA **100,** 16095–16100.

Sohn, E.J., Kim, E.S., Zhao, M., Kim, S.J., Kim, H., Kim, Y.W., Lee, Y.J., Hillmer, S., Sohn, U., Jiang, L., and Hwang, I. (2003). Rha1, an Arabidopsis Rab5 homolog, plays a critical role in the vacuolar trafficking of soluble cargo proteins. Plant Cell **15,** 1057–1070.

Stack, J.H., and Emr, S.D. (1994). Vps34p required for yeast vacuolar protein sorting is a multiple specificity kinase that exhibits both protein kinase and phosphatidylinositol-specific PI 3-kinase activities. J. Biol. Chem. **269,** 31552–31562.

Thelen, M., Wymann, M.P., and Langen, H. (1994). Wortmannin binds specifically to 1-phosphatidylinositol 3-kinase while inhibiting guanine nucleotide-binding protein-coupled receptor signaling in neutrophil leukocytes. Proc. Natl. Acad. Sci. USA **91,** 4960–4964.

Törmäkangas, K., Hadlington, J.L., Pimpl, P., Hillmer, S., Brandizzi, F., Teeri, T.H., Denecke, J. (2001). A vacuolar sorting domain may also influence the way in which proteins leave the endoplasmic reticulum. Plant Cell **13,** 2021–2032.

Toyooka, K., Okamoto, T., and Minamikawa, T. (2000). Mass transport of proform of a KDEL-tailed cysteine proteinase (SH-EP) to protein storage vacuoles by endoplasmic reticulum-derived vesicle is involved in protein mobilization in germinating seeds. J. Cell Biol. **148,** 453–463.

Tse, Y.C., Mo, B., Hillmer, S., Zhao, M., Lo, S.W., Robinson, D.G., and Jiang, L. (2004). Identification of multivesicular bodies as prevacuolar compartments in *Nicotiana tabacum* BY-2 cells. Plant Cell **16,** 672–693.

Uemura, T., Ueda, T., Ohniwa, R.L., Nakano, A., Takeyasu, K., and Sato, M.H. (2004). Systematic analysis of SNARE molecules in Arabidopsis: Dissection of the post-Golgi network in plant cells. Cell Struct. Funct. **29,** 49–65.

Watanabe, E., Shimada, T., Tamura, K., Matsushima, R., Koumoto, Y., Nishimura, M., and Hara-Nishimura, I. (2004). An ER-localized form of PV72, a seed-specific vacuolar sorting receptor, interferes the transport of an NPIR-containing proteinase in Arabidopsis leaves. Plant Cell Physiol. **45,** 9–17.